[AMERICAN JOURNAL OF SCIENCE, VOL. 295, JUNE, 1995, P. 697–741]

THERMAL HISTORY OF ROCKS: P-T-t PATHS FROM GEOSPEEDOMETRY, PETROLOGIC DATA, AND INVERSE THEORY TECHNIQUES

ANTONIO C. LASAGA and JIANG JIANXIN
Department of Geology and Geophysics, P.O. Box 208109
Yale University
New Haven, CT 06520-8109

ABSTRACT. A new powerful method of analyzing mineral zoning data is developed which extends the power of geospeedometry using inverse theory to extract complex tectonic and thermal histories from the geologic record. The theory is first tested with simple models of thermal histories. The theory is then applied to complex thermal histories involving both heating and cooling during contact and cooling during regional metamorphism. The extracted thermal histories are compared with the known thermal histories from the forward model calculations. The new technique is then tested on field data obtained from the Cortlandt Complex aureole in southeastern New York.

INTRODUCTION

There has been much interest in the past few years in applying geothermometers and geobarometers to deduce P-T paths from chemical zoning data in such minerals as garnets (Spear, 1992; Rubenach, 1992; Bergman, 1992; Hansen, 1992; Spear and others, 1991; Frost and Tracy, 1991; Anovitz, 1991; Lamb, Brown, and Valley, 1991; Motoyoshi, Thost, and Hensen, 1991; Clarke and Powell, 1991; Nichols and Berry, 1991; Spear and other, 1991; Perchuk, Gerya, and Nozhkin, 1989; Tournon, Triboulet, and Azema, 1989; Ernst, 1988; Goffe and others, 1988; Spear and Rumble, 1986; Selverstone and Spear, 1985; Selverstone and others, 1984; Spear and others, 1984; Thompson and England, 1984; Spear and Selverstone, 1983). These paths have been compared to simple tectonic models of overthrusting, crustal thickening, burial, and erosion (England and Thompson, 1984). The inclusion of geospeedometry (Lasaga, 1983) and the effect of diffusion on these calculations have been also addressed (Jiang and Lasaga, 1990; Spear, 1988, 1991; Florence and Spear, 1991). Nonetheless, these calculations yield only P-T points, and so time can only be incorporated by some type of dating technique as well as a kinetic treatment of "closure temperatures." There is much to do in deciphering the meaning of ages in complex terranes. Recent work using the $^{40}Ar/^{39}Ar$ analysis of minerals during heating (Richter and others, 1991; Lovera, Richter, and Harrison, 1989, 1991; Harrison, Lovera, and Heizler, 1991) has provided one avenue to extend significantly the rather crude methods based on simple "closure temperatures."

Recent applications of geospeedometry approaches have appeared in the literature (Docka, Berg, and Klewin, 1986; Smith and Barron, 1991; Sautter and Harte, 1990; Lindstrom and others, 1991). In this paper, a new approach will be presented based on extensions of the earlier development of geospeedometry. A major premise in the paper is that the available chemical data in the zonation of minerals can provide a wealth of previously untapped information on the thermal processes that took place as well as on the petrologic details such as the growth history of minerals.

The chief new contribution is the full use of inverse theoretical techniques to improve substantially the extraction of thermal histories. By combining the kinetic theory of ion-exchange processes, diffusion in minerals, and the use of inverse theory on many zoning profiles, a new technique akin to tomography is developed which will dramatically enhance our window into the tectonic processes to which rocks have been exposed. Even uncertainties in the diffusion data can be incorporated into the inversion and thereby constrain not only the thermal histories but also the diffusion coefficients.

The initial test of the theory has been carried out inverting discretized zoning data from the exact numerical solution of the diffusion kinetics under a variety of thermal regimes. The next test has been the application of the theory to contact metamorphism, where some constraints on the thermal history may be used as checks on the results. In particular, we have begun the application to rocks from the contact aureole of the Cortlandt Complex, which intruded regionally metamorphosed rocks in the waning stages of the Taconic orogeny. The thermal histories obtained using the new technique are consistent with the observed size of the intrusion, although the new tool changes our view of the growth of the garnets near the Cortlandt Complex.

BASIC KINETIC EQUATIONS

One of the most important properties of the technique developed here is the knowledge of the correct equations governing the kinetics. This property is in contrast with other important techniques that require understanding the nucleation and growth behavior (implicitly the possibility of equilibrium) of complex mineral reactions. The chemistry is based on the use of classical geothermometers as **continuous** recorders of the thermal history of rocks.

Let us consider two minerals (A, B) which can exchange cations 1 and 2 between them, and let us assume that the minerals are in grain boundary contact and therefore maintain local thermodynamic equilibrium. At a given temperature (and pressure), then, the concentration of components 1 and 2 at the boundary of each of the minerals will have to satisfy the equation:

$$K_{eq} = \frac{c_{A1}(0)/c_{A2}(0)}{c_{B1}(0)/c_{B2}(0)} \tag{1}$$

Because the systems studied here are good geothermometers, the value of K_{eq} in eq (1) will be a strong function of temperature. (Note that K_{eq} in eq 1 is usually defined using concentrations and not activities. However, in most cases, the non-ideal behavior is not sufficient to cause K_{eq} to vary much within typical ranges of compositional variations). If the ΔH_r of the exchange reaction remains reasonably constant, it is possible to write,

$$K_{eq} = K_0 \, exp\left(-\frac{\Delta H_r}{R}\left(\frac{1}{T} - \frac{1}{T_0}\right)\right) \tag{2}$$

where the value of K_{eq} at the arbitrary reference temperature, T_0, has been labeled K_0.

As the temperature varies during the tectonic history of a rock, K_{eq} will also vary. In turn, this variation causes all the boundary concentration values of the two minerals to change with time. This time variation of the concentration at the boundary immediately leads to diffusion of cations toward or away from the mineral edge. Therefore, the chemical evolution of the system must incorporate equations:

$$\frac{\partial c_A}{\partial t} = D_A(t)\,\frac{\partial^2 c_A}{\partial x^2} \tag{3}$$

$$\frac{\partial c_B}{\partial t} = D_B(t)\,\frac{\partial^2 c_B}{\partial x^2} \tag{4}$$

which account for the cation movement within the crystals. Of course, these equations can be generalized to include multi-component diffusion (Lasaga, 1979).

Diffusion coefficients in minerals have very high activation energies (Lasaga, 1981; Freer, 1981). Therefore, the D's in eqs (3) and (4) will vary by several orders of magnitude as the temperature changes a few hundred degrees. In fact, it is this strong variation of D with temperature that forms the basis for the technique being developed in this and subsequent papers. In general, we can introduce a reference temperature, T_0, and use the value of D at that temperature, D_0, to write the time variation of D as:

$$D(t) = D_0 d(t) \tag{5}$$

where, from the Arrhenius equation, $d(t)$ will be given by

$$d(t) = exp\left[-\frac{E_a}{R}\left(\frac{1}{T} - \frac{1}{T_0}\right)\right] \tag{6}$$

Given some thermal history, T(t), and an initial zoning profile for the exchangeable ions in a pair of adjacent minerals, these equations can be readily solved by finite difference methods. In any thermal history, the temperature will ultimately drop to low values (for example, in our case temperatures less than 300°C). Once this happens, the profiles at distances of 1 μ or more from the interface will cease to evolve even on a billion year time scale. This final zoning profile will be termed the "quenched" zoning profile and is the primary focus of interest in the development of this paper.

The fundamental question raised here is the degree to which the details of the thermal history have been preserved in the quenched zoning profile. This question is a typical one in the area of inverse theory, and we shall return to its full answer after the next section.

Simple models.—If the quenched zoning profiles are to be good indicators of the thermal history, the "shape" of the profiles should be rather sensitive to the details of the thermal history. It is best to include some simple forward modeling calculations to illustrate the sensitivity of the zoning profile to T(t). This sensitivity will, of course, be quite desirable in the process of inverting the problem. Two models will exhibit the sensitivity. One is a simple conductive model for the cooling of an intrusive. The other is a regional metamorphic model for the burial and uplift of a rock.

The intrusive model is taken to be a simple slab (see fig. 1) of half-thickness **a** with an initial temperature T_I. The country rock is taken to be initially at temperature, T_R. At any position, x, in the country rock the thermal history will therefore be given by the analytic solution:

$$T(t) = T_R + \frac{1}{2}(T_I - T_R) \cdot \left[erf\left(\frac{x+a}{2\sqrt{\kappa t}}\right) - erf\left(\frac{x-a}{2\sqrt{\kappa t}}\right) \right] \qquad (7)$$

where κ is the thermal diffusivity of the rock. The thermal history will vary with the parameters, T_R, T_I, a, and x. Suppose that the "real" thermal history was that resulting from the parameter values: T_R = 300°C, T_I = 1175°C, a = 1000 m, and x = 50 m from the contact. The thermal history is given in figure 2. The quenched zoning profile resulting from this thermal history is given in figure 3 for the case of a garnet of

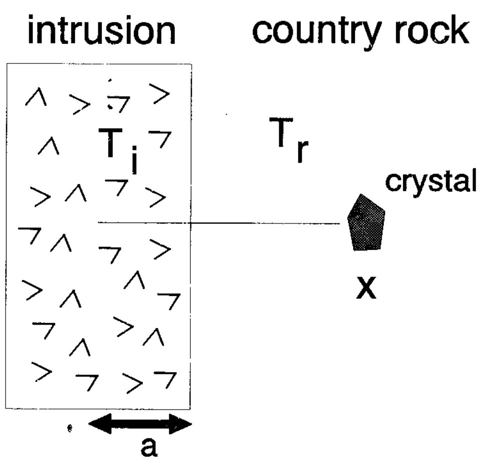

Fig. 1. Model of a contact metamorphic event. The thermal history will be a function of the distance from the contact, x, the size of the pluton, a, the initial intrusion temperature, T_i, and the initial temperature of the country rock, T_r.

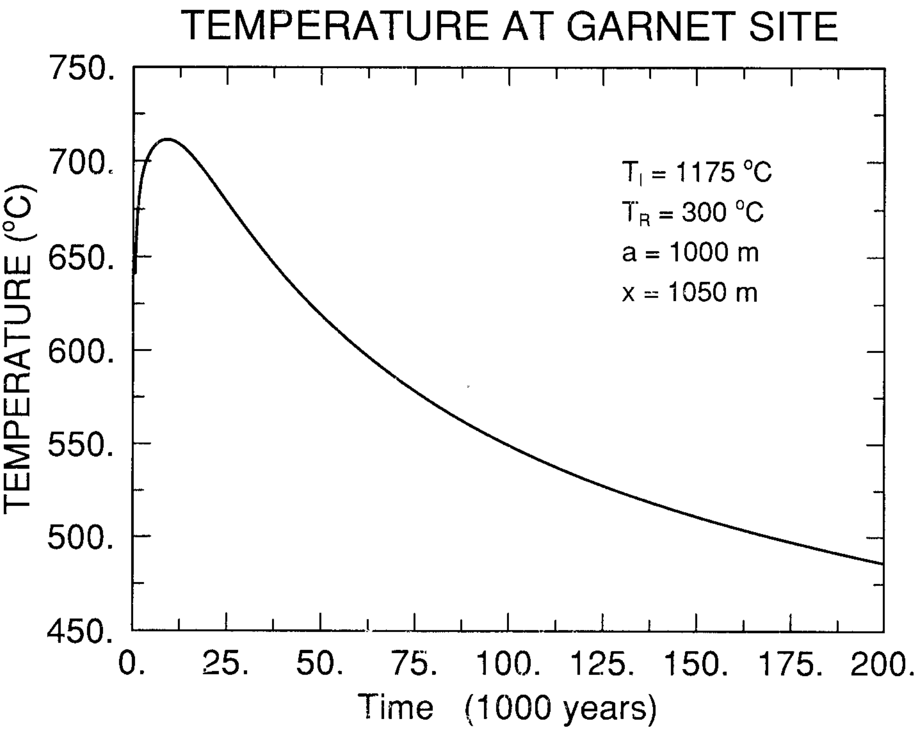

Fig. 2. Temperature-time plot for the contact metamorphism of a rock sample 50 m from the contact with a pluton of half-width, a = 1000 m, and with T_i = 1175°C and T_r = 300°C.

radius 210 μ in contact with a biotite with a radius of 525 μ (K_D of Ferry and Spear, 1978). The interesting question then is the amount of information stored in this given profile. In other words what is the degree of deviation from this given profile of a new calculated profile based on variations in the thermal history parameters. For example, the distance from the contact or the initial country rock temperature may be different, generating a different thermal history and a different quenched zoning profile. If one were to measure the zoning profile in the garnet with a microprobe, the result would be a discretization of the data shown in figure 3. Let us assume that the scan analyzed the profile in figure 3 in intervals of 5 μ for a total distance of 100 μ away from the contact, a total of 20 points. This "measured" profile will be compared with the calculated profile using different thermal histories. To compare the profiles we need to define a penalty function:

$$J \equiv \sum_{i=1}^{20} [C_i^{meas} - C_i^{calc}]^2 \tag{8}$$

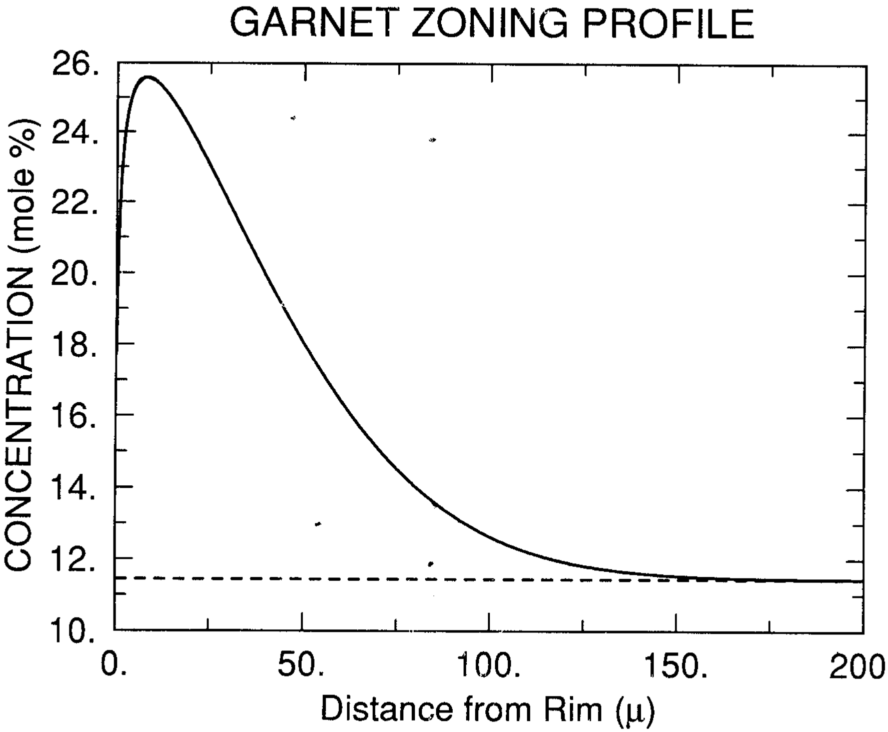

Fig. 3. Magnesium zoning profile in a garnet grain that underwent the thermal history shown in figure 2. The garnet is assumed to be 210 microns in length and to be adjacent to a biotite with a width of 525 microns.

where C^{meas} corresponds to the "exact" (that is, T = 300°C and a distance of 50 m from contact) measured profile and C^{calc} to the profile calculated from the particular values of T_R and distance from the contact assumed in the new thermal history. The next task is to determine whether the value of J is high enough to claim that the thermal history used in obtaining C^{calc} could **not** be the same as the one that gave rise to the "measured" profile. If the microprobe data have a certain inherent error in the concentration (for example, 0.2 mole percent Mg), ΔC_{probe}, then the critical value of J used to decide the significance of the deviation is given by:

$$J_{crit} = N\Delta C^2_{probe} \tag{9}$$

where N is the number of points in the profile. For example, for 20 points and a ΔC_{probe} of 0.2 mole percent, $J_{crit} = 0.8$. (Note that other values of N and other error bars will produce different values of J_{crit}.) Therefore, if a thermal history produces a profile that in comparison with the "measured" profile has a J value of 0.5, then it is possible that such a thermal history could have produced the observed profile. On the other hand, if values of J on the order of 10 are obtained, the two profiles are definitely different and the thermal history can be ruled out with confidence. Figure 4 gives a contour plot of the values of J obtained by varying the distance from the contact and the country rock temperature, T_R, away from the values used in generating the "measured" profile. The important point to note from figure 4 is the rapid increase in J above the critical value for 20 points. In fact, based on the J contours, the thermal history would be known to an accuracy close to the 0.0 contour (that is, in the middle) shown in the figure.

A similar calculation can be done for a regional metamorphism example. Using the simple uplift model of Lasaga (1983) (fig. 5), the

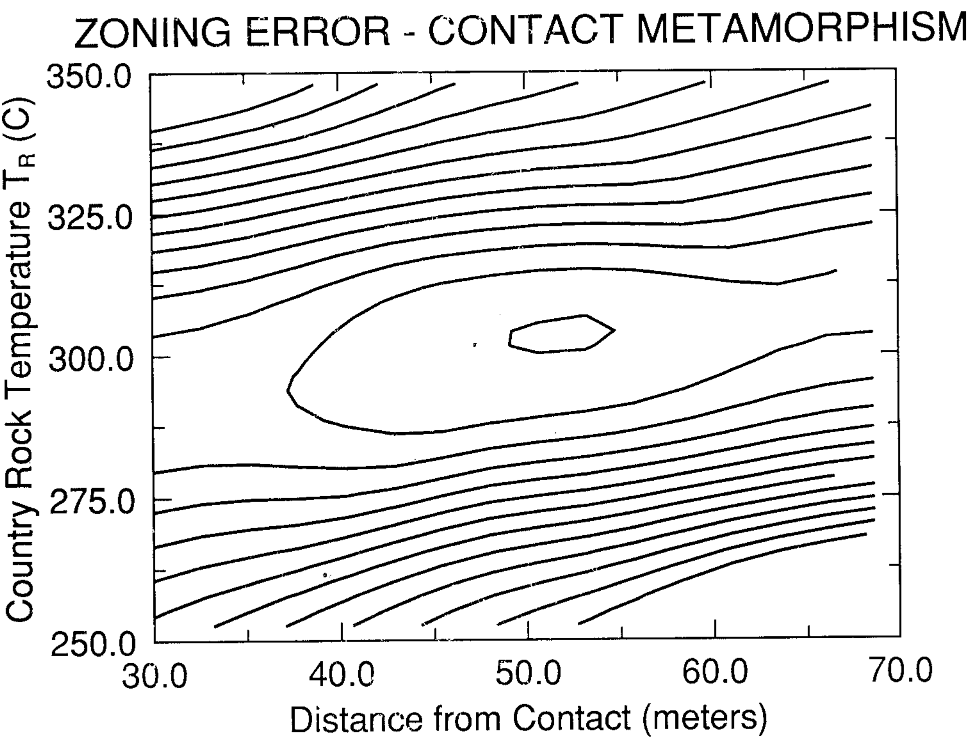

Fig. 4. Contour plot of the difference between the concentrations of 20 points in a zoning profile. Contour intervals are in units of 10 ((mole/%)^2). A standard profile is set at the "exact" value of 50 m from the contact and 300°C for the initial country rock temperature. The other profile is computed assuming different distances and temperatures. The plot shows the difference in the two concentrations squared for 20 distances from the rim of a garnet. Based on the accuracy of the microprobe, two profiles with a difference greater than 2 on this contour plot would be regarded as "different," that is, the thermal parameters can be resolved quite accurately.

temperature history now becomes:

$$T(t) = T_m \frac{1 - Ae^{(v_z^2/\kappa)t}}{1 - A} \tag{10}$$

where

$$A \equiv exp\ (-v_z z_m/\kappa)$$

T_m is the mantle temperature at the bottom of the figure, v_z is the uplift rate, z_m is the depth of the layer, and κ is the thermal diffusivity. In a similar fashion, an "exact" (that is, measured) profile can be calculated assuming the parameters, z_m = 25 km, v_z = 3.0 mm/yr, and T_m = 650°C. Figure 6 exhibits the temperature-depth path taken by the mineral assemblage. If a 210 μ radius garnet exchanges with a 525 μ radius biotite according to the K_D (Ferry and Spear, 1978):

$$K_D = 2.18602\ exp\ (-(2089.2 + 9.562\ P)/T)\ P\ in\ Kbars\ T\ in\ K \tag{11}$$

then figure 7 shows the resulting zoning profile. To obtain the penalty function, only 20 points will be used in the profile with a uniform spacing of 5 μ. The variation of the penalty function, J, with the variables, T_m and v_z is given in figure 8. Recall that J_{crit} = 0.8 for 20 points. Therefore, once more the zoning profile can narrow down the possible thermal histories in these simple models.

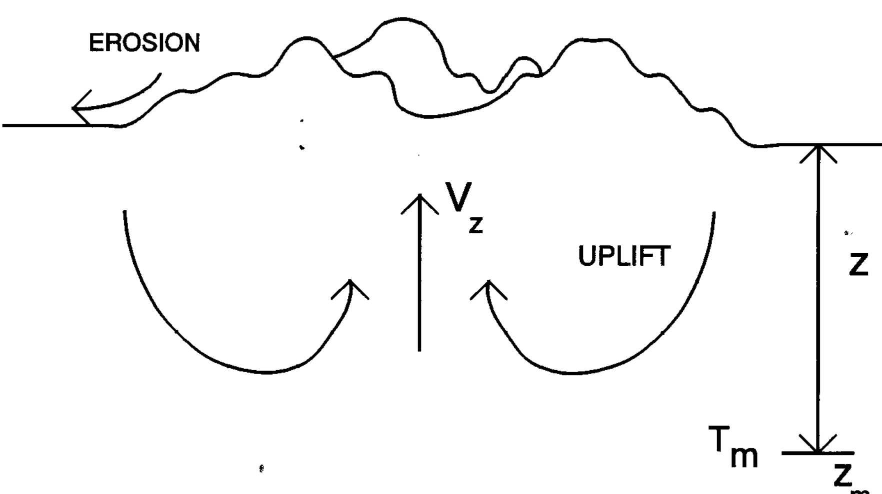

Fig. 5. Regional metamorphism model. A constant uplift rate of v_z is assumed due to erosion. The temperature at depth z_m is set at T_m. The temperature profile is assumed to be at steady state (see Lasaga, 1983).

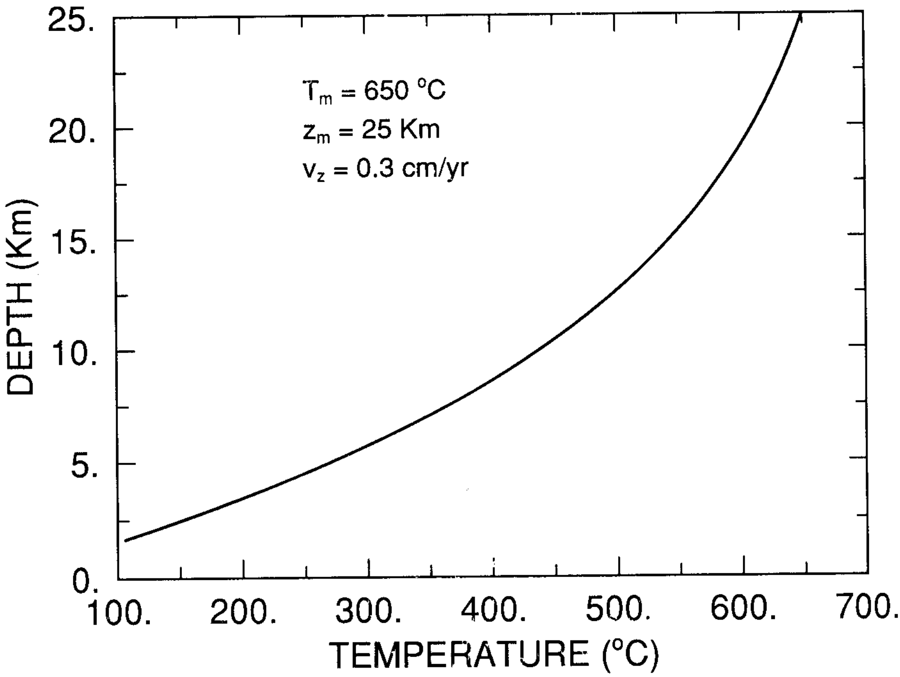

Fig. 6. Temperature-depth (P-T) path followed by the mineral assemblage using the model in figure 5 and the parameters $z_m = 25$ km, $v_z = 3.0$ mm/yr, and $T_m = 650$ C .

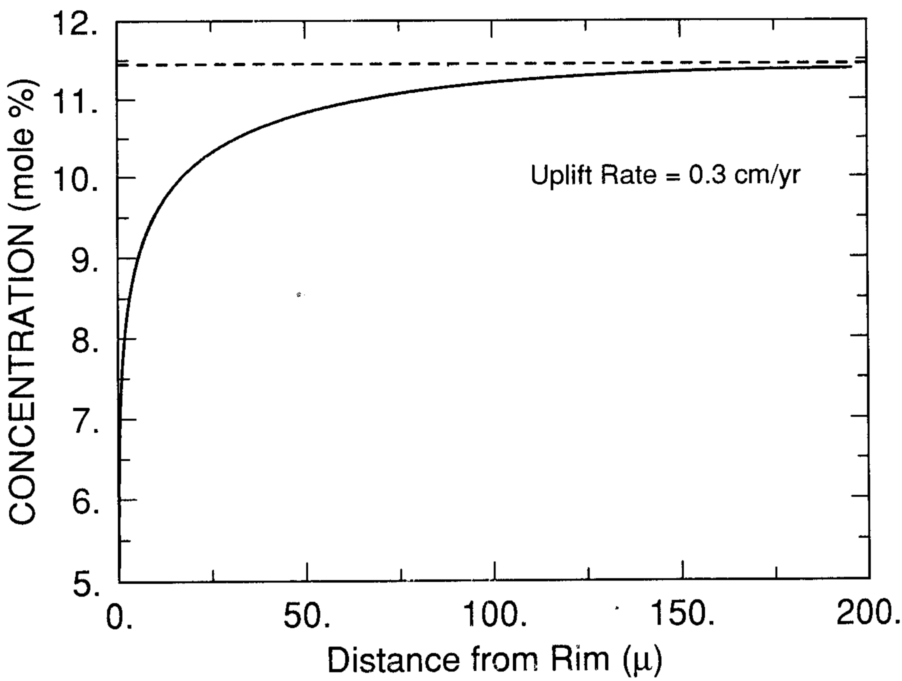

Fig. 7. The magnesium zoning profile in a garnet of 210 microns length adjacent to a biotite 525 microns in diameter. The thermal history used correspond to the P-T-t path in figure 6.

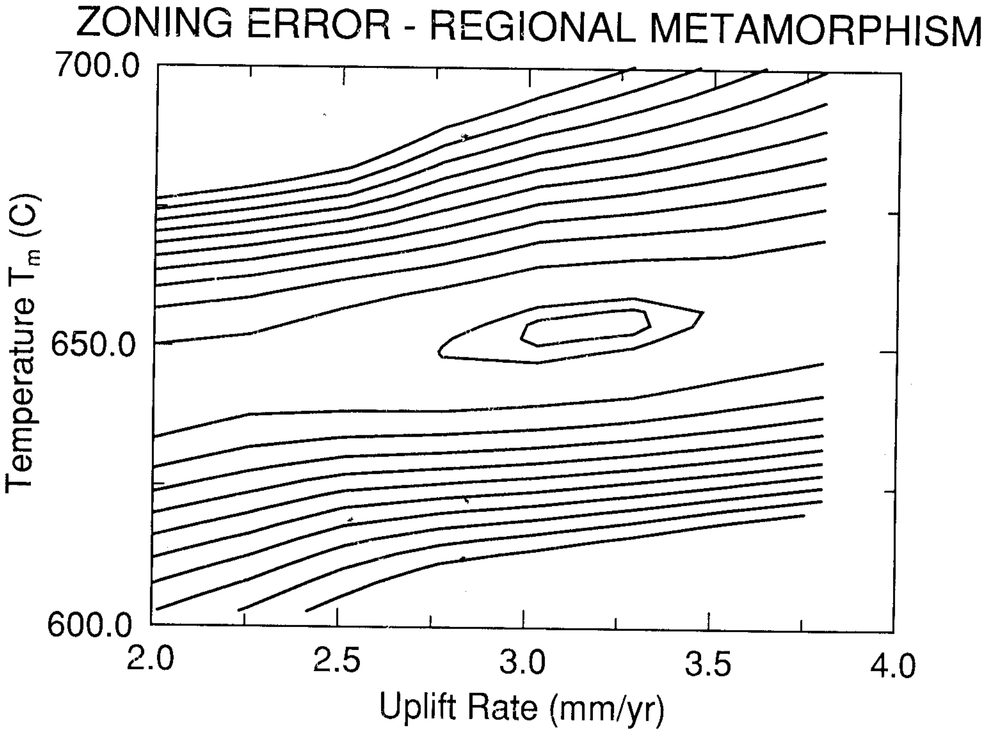

Fig. 8. Same as figure 4. In this case the "exact" profile assumed an uplift rate of 3 mm/yr and a temperature, T_m = 650 C. The contour interval in this case is 3 (mole/%)^2.

GENERAL SOLUTIONS

The best method of dealing with the time variation of D in eqs (3) and (4) is to introduce the new time variable, t′ (Lasaga, 1983):

$$t' \equiv \int_0^t d(\tau)d\tau \tag{12}$$

Use of this t′ simplifies the diffusion equations:

$$\frac{\partial c_A}{\partial t'_A} = D_{A0}\frac{\partial^2 c_A}{\partial x^2} \tag{13}$$

$$\frac{\partial c_B}{\partial t'_B} = D_{B0}\frac{\partial^2 c_B}{\partial x^2} \tag{14}$$

Note that there are two different t′ scales, one for each mineral. Each of the last diffusion equations is trivial to solve, **if** we know the boundary condition for the concentration as a function of **t′**, $g_A(t'_A)$ or $g_B(t'_B)$ using the appropiate t′ scale. If we write the initial concentration variation as

$c^I(x)$, then the solution of (13) or (14) for any given mineral (we drop the A and B) is given by

$$c(x, t) = c(x, t') = \frac{x}{2\sqrt{\pi D_0}} \int_0^{t'} g(\tau') \frac{exp\left(-\dfrac{x^2}{4D_0(t' - \tau')}\right)}{(t' - \tau')^{3/2}} d\tau' + \frac{1}{2\sqrt{\pi D_0 t'}} \int_0^{\infty} c^I(x')\,[e^{-(x-x')^2/4D_0t'} - e^{-(x+x')^2/4D_0t'}]dx' \quad (15)$$

(Eq 15 can be obtained by using Laplace transforms to solve the diffusion equation.) In most cases, a very good approximation for the systems with which we will be dealing is to set $c^I(x)$ = constant = c^I. In this case the last term in eq (15) simplifies and the equation reduces to

$$c(x,t) = c(x,t') = \frac{x}{2\sqrt{\pi D_0}} \int_0^{t'} g(\tau') \frac{exp\left(-\dfrac{x^2}{4D_0(t' - \tau')}\right)}{(t' - \tau')^{3/2}} d\tau' + c^I erf\left(\frac{x}{2\sqrt{D_0 t'}}\right) \quad (16)$$

Measured profiles are based on the final quenched zoning profiles, and so the appropiate equation needed is:

$$c(x) = c(x, t'_\infty) = \frac{x}{2\sqrt{\pi D_0}} \int_0^{t'_\infty} g(\tau') \frac{exp\left(-\dfrac{x^2}{4D_0(t'_\infty - \tau')}\right)}{(t'_\infty - \tau')^{3/2}} d\tau' + c^I erf\left(\frac{x}{2\sqrt{D_0 t'_\infty}}\right) \quad (17)$$

where the number t'_∞ is the final (quenched) value of the t' parameter,

$$t'_\infty = \int_0^\infty d(\tau)d\tau \quad (18)$$

In a nutshell, our task is to extract from measured zoning profiles, $c(x_i)$, and eq (17) the boundary concentration function $g(t')$ and then to extract from $g(t')$ the thermal evolution, $T(t)$.

There are several approaches to inverting eq (17) for $g(t')$. We will present three different methods in this paper, each with its own strengths and weaknesses.

For some problems with underdetermination, the Backus-Gilbert inverse may be useful (Tarantola, 1987). In this case, we build the solution by approximating a delta function from the various kernels in eq (18). The end result is that if we define,

$$\bar{c}_i = c(x_i) - c^I erf\left(\frac{x_i}{2\sqrt{D_0 t'_\infty}}\right). \quad (19)$$

then, from the previous equation,

$$\bar{c}_i = \frac{x_i}{2\sqrt{\pi D_0}} \int_0^{t'_\infty} g(\tau') \frac{exp\left(-\dfrac{x_i^2}{4D_0(t'_\infty - \tau')}\right)}{(t'_\infty - \tau')^{3/2}} d\tau' \tag{20}$$

which we can rewrite as

$$\bar{c}_i = \int_0^{t'_\infty} g(\tau')K_i(\tau')d\tau' \tag{21}$$

where the K_i are known and equal to

$$K_i(\tau') = \frac{x_i}{2\sqrt{\pi D_0}} \frac{exp\left(-\dfrac{x_i^2}{4D_0(t'_\infty - \tau')}\right)}{(t'_\infty - \tau')^{3/2}} \tag{22}$$

In the Backus-Gilbert method, the value of the function g(t′) at some particular value of t′, t'_0, is written as a combination of the known data values, $\bar{c}_i$, that is,

$$g(t'_0) = \sum_i q_i(t'_0)\bar{c}_i \tag{23}$$

Note that the unknown coefficients, q_i, depend on the value of t'_0. Thus while relation (23) is a linear one between the data points and g, the function q(t′) can be quite complex to adjust to any complex g(t′) function. Using eq (21) the last expression may be rewritten as

$$g(t'_0) = \int_0^{t'_\infty} g(t') \left[\sum_i q_i(t'_0)K_i(t')\right] dt' \tag{24}$$

where the function K_i is defined by eq (22). The trick involves picking the q_i so that the summation inside brackets in eq (24) approximates a delta function (hence making the equality true), that is, for each value of t'_0 we require that:

$$\int_0^{t'_\infty} \left[\sum_i q_i(t'_0)K_i(t')\right] K_j(t')dt' = K_j(t'_0)$$

or written as algebraic equations:

$$\sum_i \left[\int_0^{t'_\infty} K_i(t')K_j(t')dt'\right] q_i(t'_0) = K_j(t'_0) \tag{25}$$

which can be written in matrix form as:

$$\sum_i S_{ji}q_i(t'_0) = K_j(t'_0) \tag{26}$$

with the matrix S defined by the integral in eq (25). Inserting the expressions for K_i into eq (25) and evaluating the integral in (25) leads to an expression for the matrix S:

$$S_{ji} = \frac{4x_i x_j D_0}{\pi(x_i^2 + x_j^2)^2}\left(\frac{x_i^2 + x_j^2}{4D_0 t'_\infty} + 1\right) exp\left(-\frac{x_i^2 + x_j^2}{4D_0 t'_\infty}\right) \tag{27}$$

We can solve the matrix eq (26) for q_i and insert q_i into eq (23) to obtain a solution for $g(t'_0)$:

$$g(t'_0) = \sum_{i=1}^{N} \frac{x_i}{2\sqrt{\pi D_0}} \frac{exp\left(-\dfrac{x_i^2}{4D_0(t'_\infty - t'_0)}\right)}{(t'_\infty - t'_0)^{3/2}} \sum_{j=1}^{N} (S^{-1})_{ij}\, \bar{c}_j \tag{28}$$

where S^{-1} is the inverse of the matrix S. Note that in this and subsequent methods, there are two constants that appear: D_0 and t'_∞. D_0 is arbitrary, although it is usual to set it as the value of D near the highest temperature in the thermal history. In any case, once D_0 is picked, then t'_∞ is not arbitrary but is a parameter that can be estimated (from the profiles) and refined in the inversion. However, if a rough approximation to the value of t'_∞ is used, the inversion will usually work well.

We can test the use of the Backus-Gilbert method in some of the contact and regional metamorphic examples discussed earlier. For example, the thermal history of a garnet 25 m from the contact with an intrusion of 800 m half-width and an initial temperature of 1175°C is given in figure 9. The country rock is assumed to be initially 300°C. The profile generated in the garnet is given in figure 10 and assumes the garnet is next to a biotite. The diffusion data of Cygan and Lasaga (1985) and the K_D data of Ferry and Spear (1978) are used assuming P = 1 kb. The garnet is initially homogeneous with X_{Mg} = 11.45 mole percent. Only the iron and magnesium are allowed to vary. The t′ values can be computed for the garnet from the diffusion coefficient and the thermal history using the equation

$$t' = \int_0^t D(T(t))/D_0 dt \tag{29}$$

where D_0 was arbitrarily set at 0.01 μ^2/yr. Figure 11 plots the boundary concentration of Mg as a function of both t and t′, the latter being our g(t′) function. The key question is how well we can obtain this known g(t′) from the data in the final (quenched) zoning profile (fig. 10). Because the actual field data in any application would be in the form of discrete analysis from a microprobe or TEM traverse, 35 points were selected from figure 10, and these points were considered as data for the Backus-Gilbert method. The points were selected with a 0.5 μ spacing up to a distance of 5 μ, with a spacing of 1 μ up to a distance of 10 μ and with a spacing of 2 μ up to 20 μ; after a distance of 20 μ, the spacing was

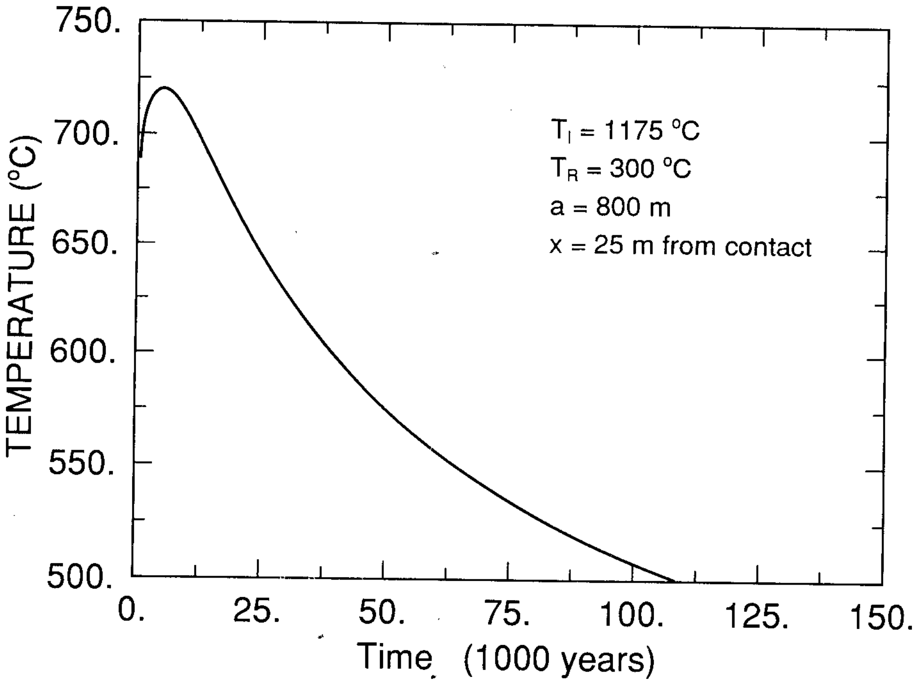

Fig. 9. Contact thermal history for a sample 25 m from an intrusion that has a half-width of 800 m and with parameters T_i = 1175°C and T_r = 300°C (see fig. 1).

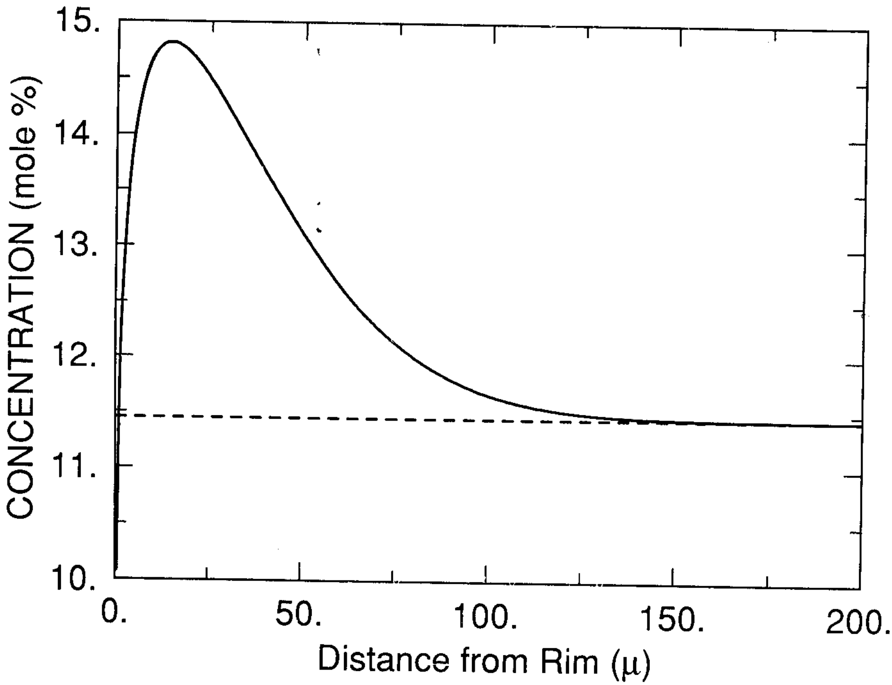

Fig. 10. Magnesium zoning profile in garnet exposed to the thermal history shown in figure 9. Garnet is assumed to be next to a biotite, and the sizes of the garnet and biotite are 210 and 525 microns respectively.

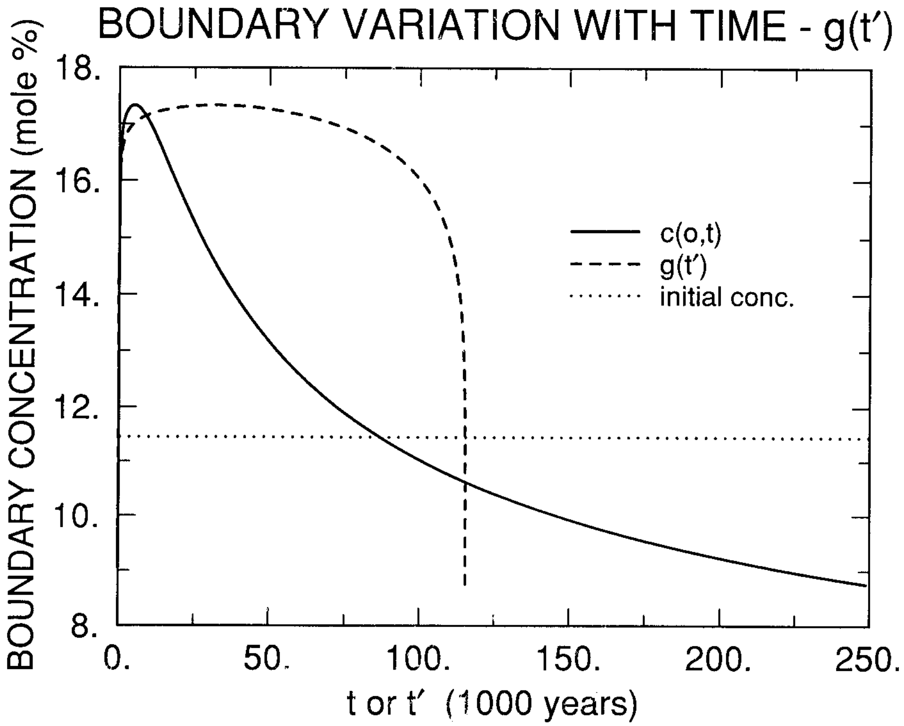

Fig. 11. Boundary concentration of magnesium (in mole percent) as a function of time for the garnet discussed in figure 10. One curve gives the concentration as a function of t′ and abruptly falls off as the limiting value of t′ is approached (t_∞). The other curve shows the concentration as a function of regular time.

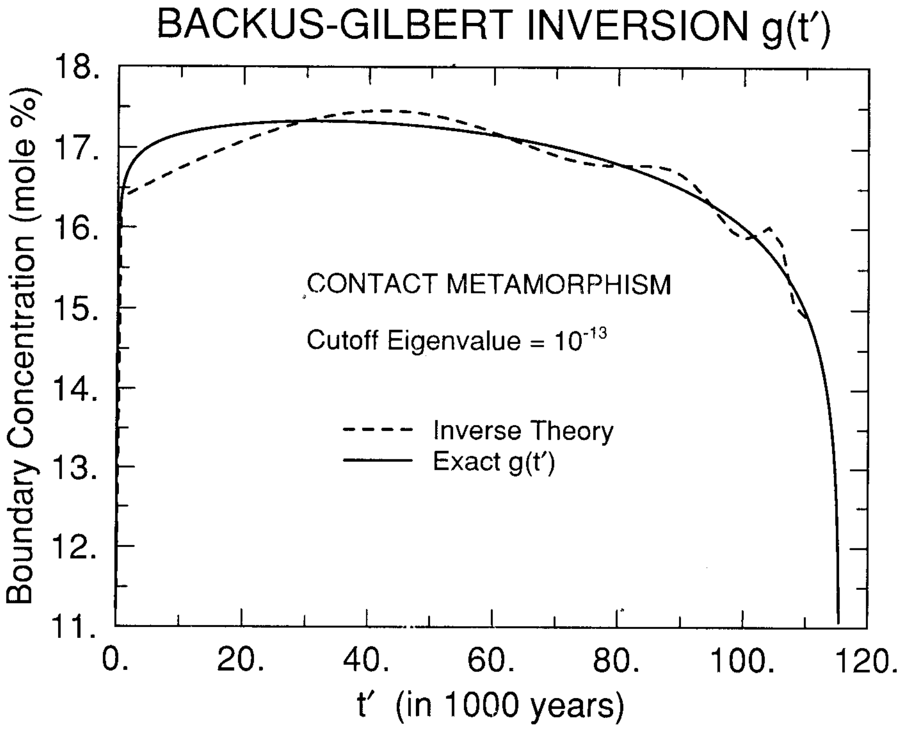

Fig. 12. Inversion of the discretized zoning profile from figure 10 using the Backus-Gilbert method and most eigenvalues. The plot gives the inverted boundary concentration as a function of t′ and compares it with the exact boundary variation (fig. 11). Note that if the inversion of the S matrix is done with all eigenvalues, oscillatory solutions result.

broader, that is, 5 to 10 μ. We found that in inverting the S matrix, care must be taken to exclude very small eigenvalues, otherwise oscillations are introduced in the solution. If S is inverted using all eigenvalues larger than 10^{-13}, then the extracted g(t′) function oscillates about the true solution as shown in figure 12. However, if the eigenvalues less than 10^{-12} were ignored in inverting S, then the profile in figure 13 is obtained. In both cases, the exact g(t′) function is also plotted for comparison. Clearly, the zoning profile—even at the level of discretization forced by a microprobe—contains enough information to retrieve a g(t′) function.

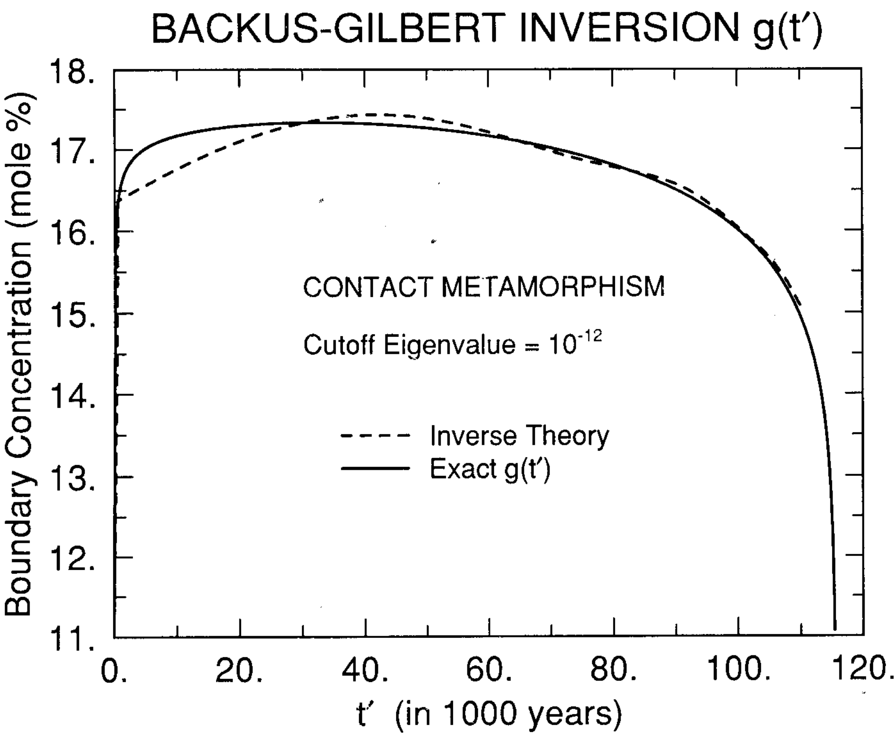

Fig. 13. Geothermometry allows us to relate the boundary concentration to temperature. Hence obtaining the boundary concentration with time leads to a thermal history. This plot compares the "exact" boundary concentration for a contact metamorphic garnet (forward modeling) with the boundary concentration extracted using the Backus-Gilbert inverse techniques. In this case, very small eigenvalues were ignored in inverting the S matrix. The concentration is plotted as a function of t′, which can be related to time.

As another example, the regional metamorphic uplift model discussed earlier can be used to obtain an appropriate thermal history. In this case, we chose the following parameters: $T_z = 600°C$, $z_m = 25$ km, $v_z =$ 3 mm/yr. This thermal history generates the garnet profile shown in figure 14. Once more, the profile is discretized using a total of 30 points,

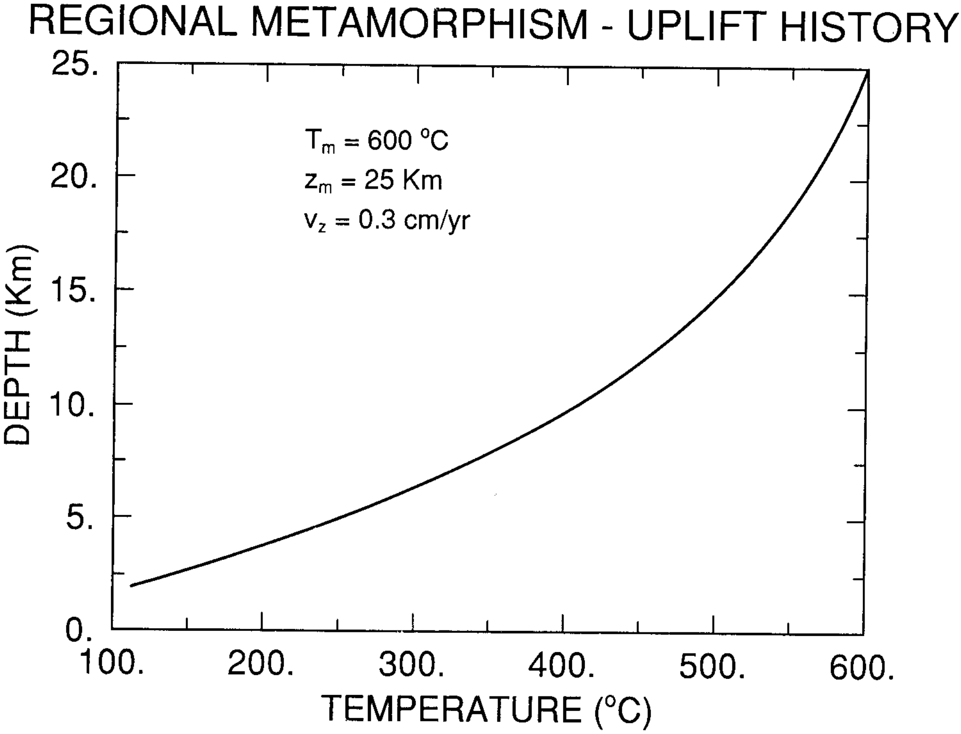

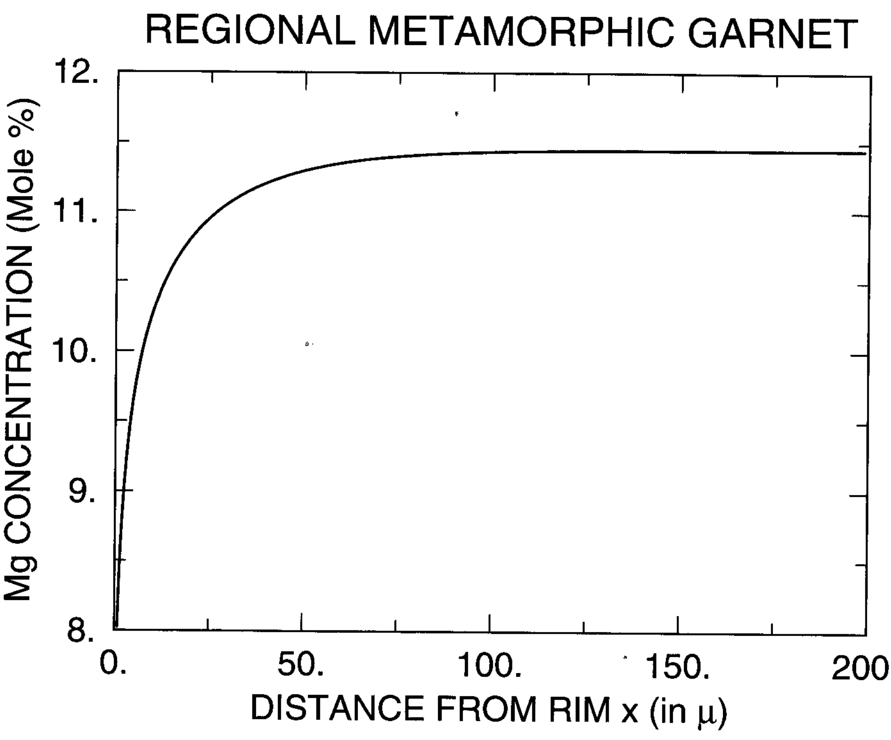

Fig. 14(A) The regional metamorphic thermal history (P-T path) obtained from the model in figure 5 using z_m = 25 Km, v_z = 3 mm/yr and T_z = 600°C.
(B) Magnesium zoning profile for a garnet experiencing such a metamorphic history.

spaced 1 μ apart close to the rim (up to a distance of 10 μ) and 5 to 10 μ apart far from the rim. The comparison of the Backus-Gilbert inversion and the exact g(t′) function are given in figure 15. Note the excellent agreement.

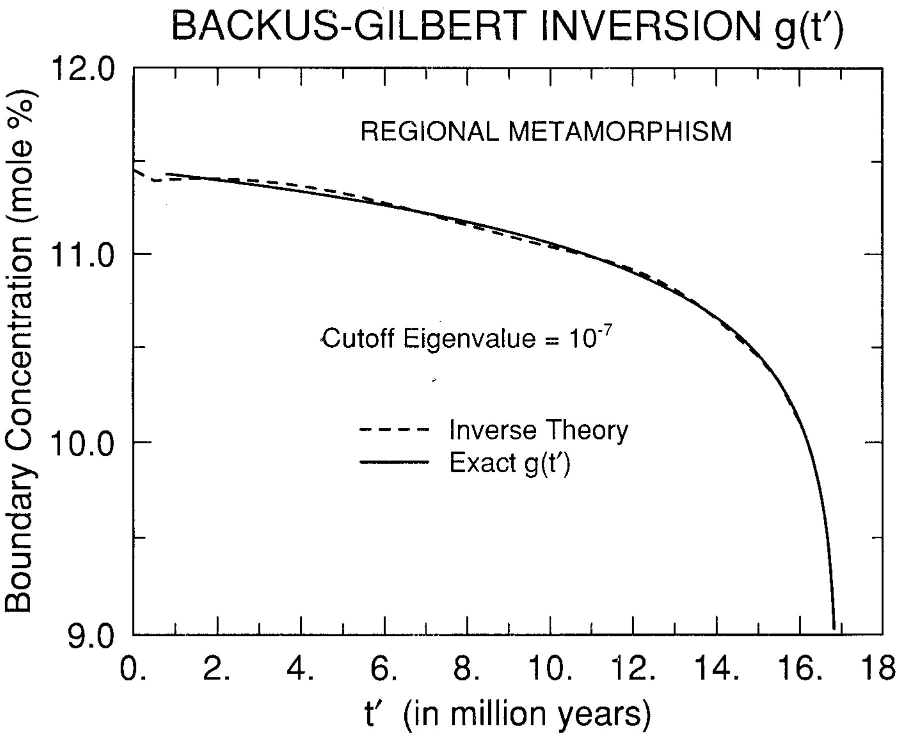

Fig. 15. Same inversion as carried out in figure 13 but for the regional metamorphic case discussed in figure 14.

It is important to emphasize that the g(t′) functions generated in both cases above were **not** constrained to use the simple models employed in generating the zoning profiles. In other words, **any** thermal history (that is, any g(t′) function) was allowed in the inversion. After eliminating very low eigenvalues, the program returned the known g(t′) function to high accuracy.

Alternatively, we can discretize the unknown function g(t′) into N segments: g(0), g(Δt′), g(2Δt′), . . . , g(N Δt′), g(t'_∞), which we can label as $g_0, g_1, g_2, \ldots, g_N, g_\infty$. We can then approximate the function g between n $\Delta t'$ and (n + 1)$\Delta t'$ by

$$g(t') = g_n + \frac{g_{n+1} - g_n}{\Delta t'}(t' - n\Delta t') \tag{30}$$

In this case, eq (17) becomes,

$$c_i = c(x_i) = \sum_j G_{ij} g_j \tag{31}$$

so that we reduce the problem to a typical matrix inverse problem with the matrix element in eq (31) given by,

$$G_{ij} = \frac{2}{\sqrt{\pi}} \int_{\gamma_{ij}}^{\gamma_{i(j+1)}} \frac{t'_\infty - (j-1)\Delta t' - \dfrac{x_i^2}{4D_0 u^2}}{\Delta t'} e^{-u^2}\, du$$

$$+ \frac{2}{\sqrt{\pi}} \int_{\gamma_{i(j+1)}}^{\gamma_{i(j+2)}} \left(1 - \frac{t'_\infty - j\Delta t' - \dfrac{x_i^2}{4D_0 u^2}}{\Delta t'} \right) e^{-u^2}\, du \tag{32}$$

where the γ's are defined by:

$$\gamma_{ij} \equiv \frac{x_i}{2\sqrt{D_0(t'_\infty - (j-1)\Delta t')}} \tag{33}$$

Note that the initial value, c^I, is also varied in this formulation (that is, $c^I = g_0$).

Once more, the inversion of the linear eq (31) needs to input some apriori knowledge of the behavior of the thermal history to obtain a reasonable constraint. (For example, the system cannot differentiate a thermal history that smoothly cools from some peak value from a thermal history that does the same thing but oscillates wildly at the same time (see fig. 16). Therefore, the wild oscillatory solutions must be eliminated. There are several ways to carry this out. We will discuss two methods used in our analysis.

The first method simply requires that the temperature always decrease or stay the same, that is,

$$g_{i+1} \geq g_i \textit{ for all } i \tag{34}$$

The program then minimizes the least squares of the data, that is, minimizes the penalty function, J, defined by:

$$J = \sum_i^n w_i (c_i - \sum_j G_{ij} g_j)^2 \tag{35}$$

The minimization is accomplished by obtaining the gradient of J and using steepest descent methods. However, if the move requires eq (34) to be violated, then the move sets the two g values equal.

An alternative method establishes a **monotonicity criterion.** This is accomplished by the addition of a function to the penalty function:

$$J = \sum_i^n w_i \left(c_i - \sum_j G_{ij} g_j \right)^2 + \epsilon \sum_j^n e^{\alpha_j (g_{j+1} - g_j)} \tag{36}$$

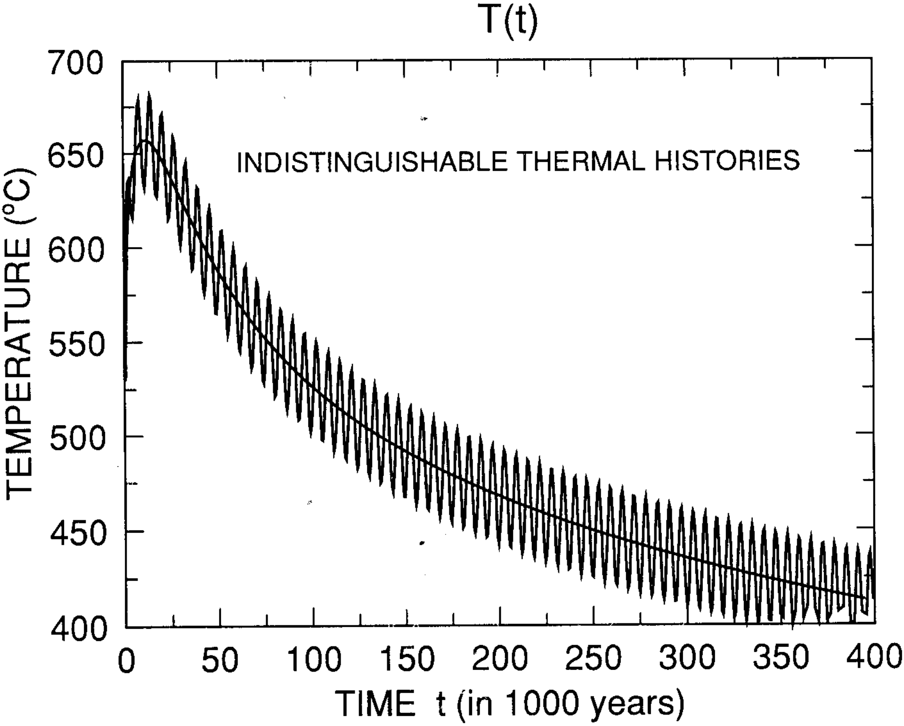

Fig. 16. Two different thermal histories, which, nonetheless, produce indistinguishable zoning profiles.

This second term is relatively innocuous if eq (34) holds true. On the other hand, if eq (34) is violated, the exponential becomes positive, and a large addition to J is penalized. This is achieved best if α is a relatively large positive number ($\epsilon = 0.1$, and $\alpha = 40$ were used).

Both methods were applied to the same regional metamorphism model used with the Backus-Gilbert method earlier. Figures 17 and 18 illustrate the fact that similar results are obtained with discretization as with the Backus-Gilbert techniques.

Another test used a different regional metamorphic history based on the parameters $T_m = 650°C$, $z_m = 25$ km, and $v_z = 3$ mm/yr. Figure 19 shows the results using the inequality criterion and discretizing the data with a spacing of 2 my except for the last 2 my where a spacing of 0.2 my was used for g(t′). Once more the results are in good agreement with the exact g(t′) function.

An even better method of proceeding may be to introduce continuous functions for g(t′) and evaluate coefficients in the functions. Because g(t′) will have a fast drop near t'_∞ (see earlier figures), a set of functions

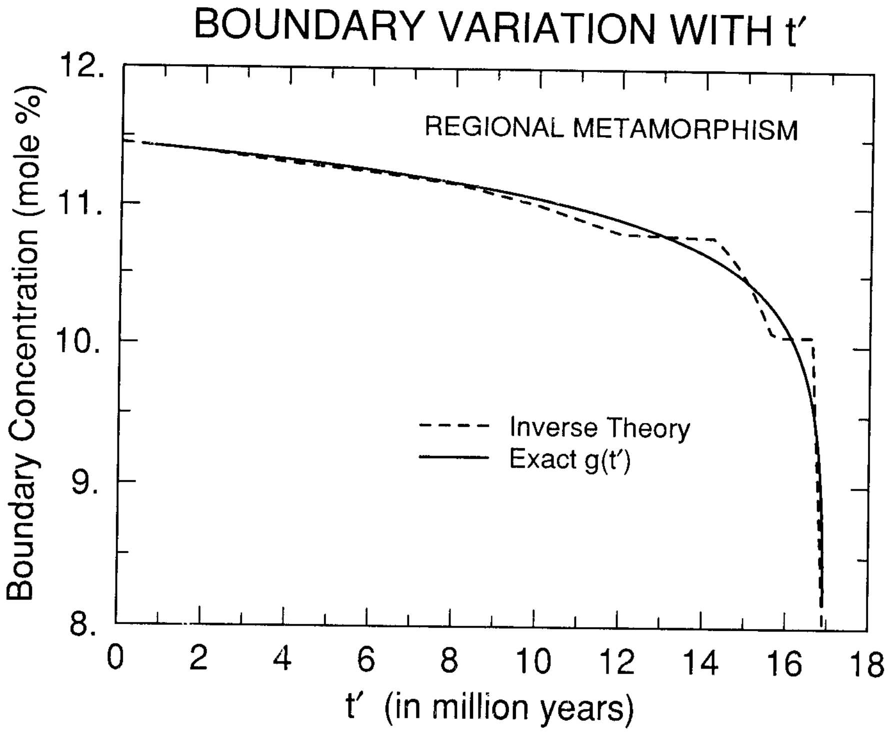

Fig. 17. Inversion of the zoning profile discussed in figure 14. The inversion now uses the discretization of the boundary concentration (into 20 segments) as a function of time followed by a minimization of the least squares error using the inequality criterion (eq 27) as discussed in the text.

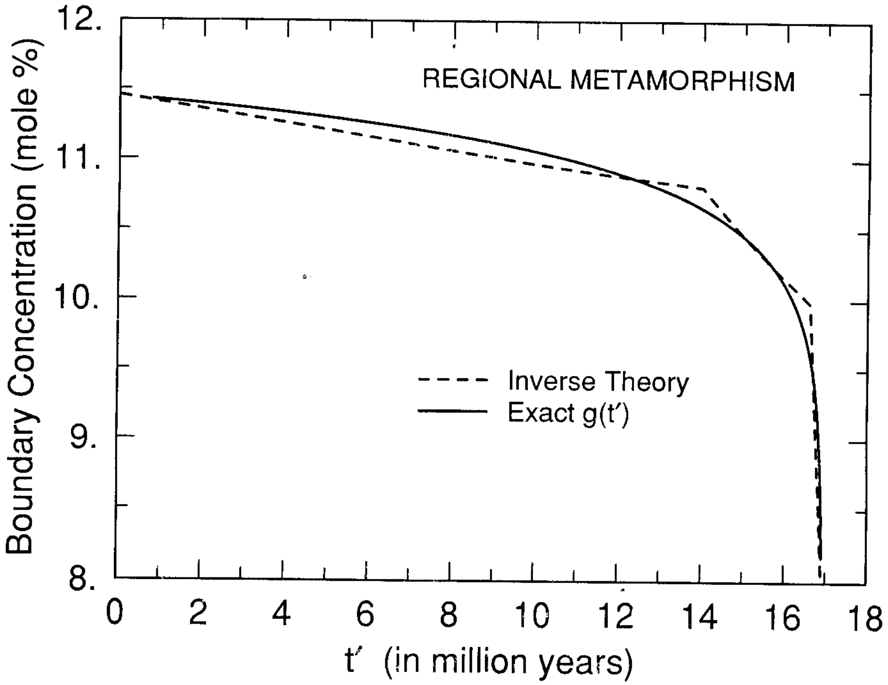

Fig. 18. Inversion of the zoning profile discussed in figure 14. The inversion now uses the discretization of the boundary concentration (into 20 segments) as a function of time followed by the minimization of the error using the monotonicity criterion as discussed in the text. The parameters used were $\epsilon = 0.1$ and $\alpha = 40$.

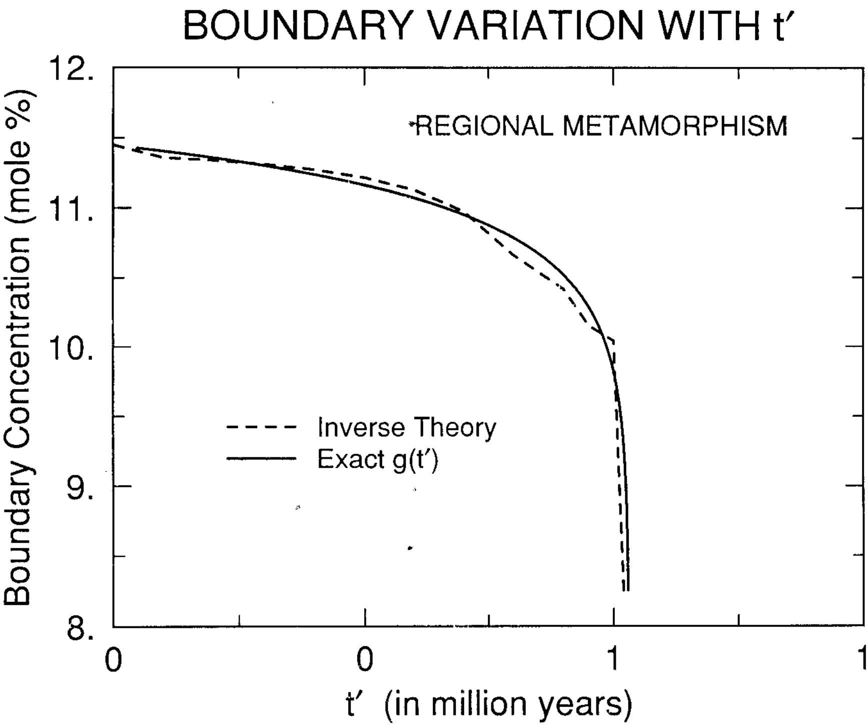

Fig. 19. Another inversion of a regional metamorphic case with the parameters, z_m = 25 km, v_z = 3 mm/yr, and T_m = 650°C. The inversion method discretizes the boundary concentration as a function of time and minimizes the least-squares error subject to the inequality condition.

that have the correct shape and thus should generally be useful for these type of inversions are:

$$g(t') = C^I + a_1 e^{-A_1/t'} + a_2 e^{-A_2/t'} + \cdots\cdots$$
$$+ b_1(e^{-B_1/(t'_\infty - t')} - e^{-B_1/t'_\infty}) + b_2(e^{-B_2/(t'_\infty - t')} - e^{-B_2/t'_\infty}) + \cdots \quad (37)$$

where the functions are such that as t' approaches 0, g approaches C^I, and as t' approaches t'_∞, g decreases sharply. If the exponents are arbitrarily picked and fixed (for example, equivalent to selecting a basis set) then the inversion merely requires that the best set of coefficients, a_i and b_i, be picked. In particular, it can be checked that the elimination of temperature "wiggles" for a cooling event merely requires that all the coefficients be **positive** in the inversion (for the case that only the B functions are present, that is, general cooling history). Therefore, this problem can be handled by the classic NonNegative Least Squares or

NNLS method (for example, Lawson and Hanson, 1974, p. 160). Inserting the expression in eq (37) for g(t′) in eq (17) results in,

$$c(x_i) = C^I + \sum_j \left[\frac{2}{\sqrt{\pi}} \int_{x_i/2\sqrt{D_0 t'_\infty}}^{\infty} exp\left(- \frac{4D_0 A_j u^2}{4D_0 u^2 t'_\infty - x_i^2} - u^2 \right) du \right] \mathbf{a_j}$$
$$+ \sum_j \left[\frac{erfc\left[\left(1 + \frac{4D_0 B_j}{x_i^2} \right)^{1/2} \frac{x_i}{2\sqrt{D_0 t'_\infty}} \right]}{\sqrt{1 + \frac{4D_0 B_j}{x_i^2}}} - erfc\left(\frac{x_i}{2\sqrt{D_0 t_\infty}} \right) e^{-B_j/t'_\infty} \right] \mathbf{b_j} \quad (38)$$

Note that with this last equation, the problem of obtaining the coefficients a_j and b_j becomes a simple problem in **linear** inversion theory. Hence, for a fixed set of A_j and B_j, the NNLS method is used to obtain a_j and b_j after computing the terms in brackets in eq (38). Returning to the metamorphic example discussed earlier, the input profile consisted of Mg content at 5, 10, 15, 18, 20, 26, 30, 40, 60, 80, 100, 120, 150, 200, and 350 μ from the rim. This profile was used in carrying out an inversion using the continuous function method. Figure 20 shows the very close agreement between the calculated and exact g(t′) for the case where only 7 B values were used (0.05, 0.1, 0.5, 1.0, 2.5, 4.0, and 6.0), and no A values were used.

An important test of the robustness of the inversion technique is to add random **noise** to the discrete profile, thereby simulating instrumental limitations. If a total error of 0.1 mole percent is added to the profile used to obtain the inversion in figure 20, the new extracted g(t′) function (using the continuous function method) is given in figure 21. Note that, indeed, the inversion is relatively unaffected by the addition of **random** noise. If three more functions with B values at 0.2, 1.5, and 3.0 were added to the basis, the result (fig. 22) is quite close to the exact g(t′) function (fig. 22A) even with the addition of random noise (fig. 22B).

Boundary condition.—To proceed further, it is essential to obtain a practical formulation for the relation between the thermal history, T(t), and the boundary concentration function g(t′) discussed above. Luckily, the previous work on geospeedometry (Lasaga, Richardson, and Holland, 1977; Lasaga, 1983) has paved the way for the required treatment. In the previous work, the thermal histories have all been rather simple. We need to extend this work, then, to encompass any complex model-independent heating and cooling function. The generalization begins with the formula obtained in Lasaga, Richardson, and Holland (1977) for the rate of change of the boundary concentration, given a cooling rate s:

$$\frac{dc_B(0,t)}{dt} = \frac{\beta}{\sqrt{D_B(t)/D_{gar}(t)}\left(\frac{1}{c^I_{Mg,gar}} + \frac{1}{c^I_{Fe,gar}} \right) + \left(\frac{1}{c^I_{Mg,B}} + \frac{1}{c^I_{Fe,B}} \right)} \quad (39)$$

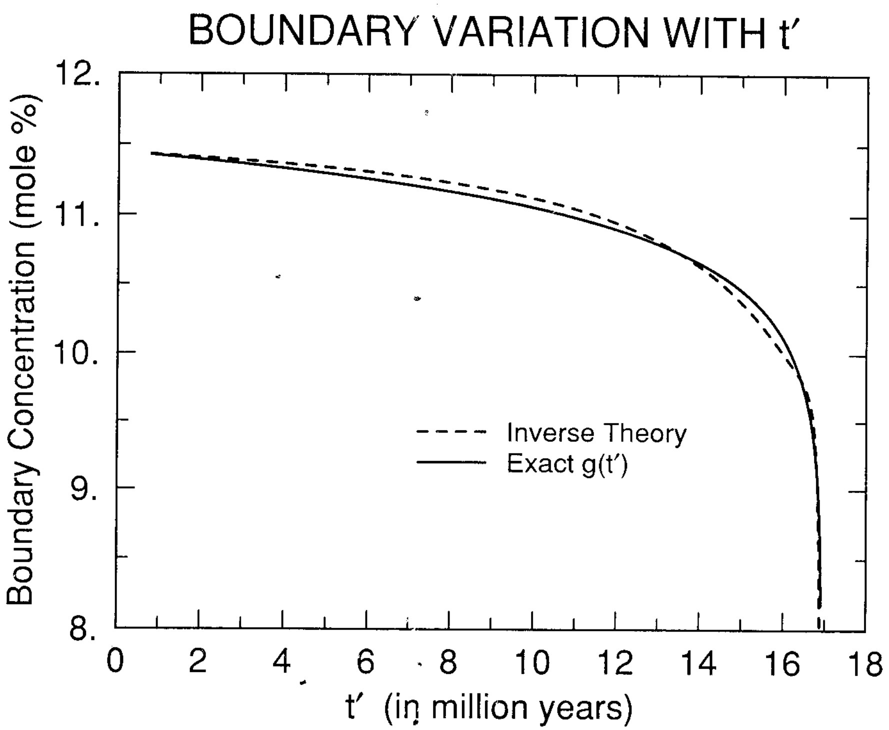

Fig. 20. Inversion of the zoning profile discussed in figure 14. The inversion now uses the continuous functions given in eq (30) and minimization of the error using the NNLS method. Seven functions were used with A = 0 and B = 0.05, 0.1, 0.5, 1.0, 2.5, 4.0, and 6.0.

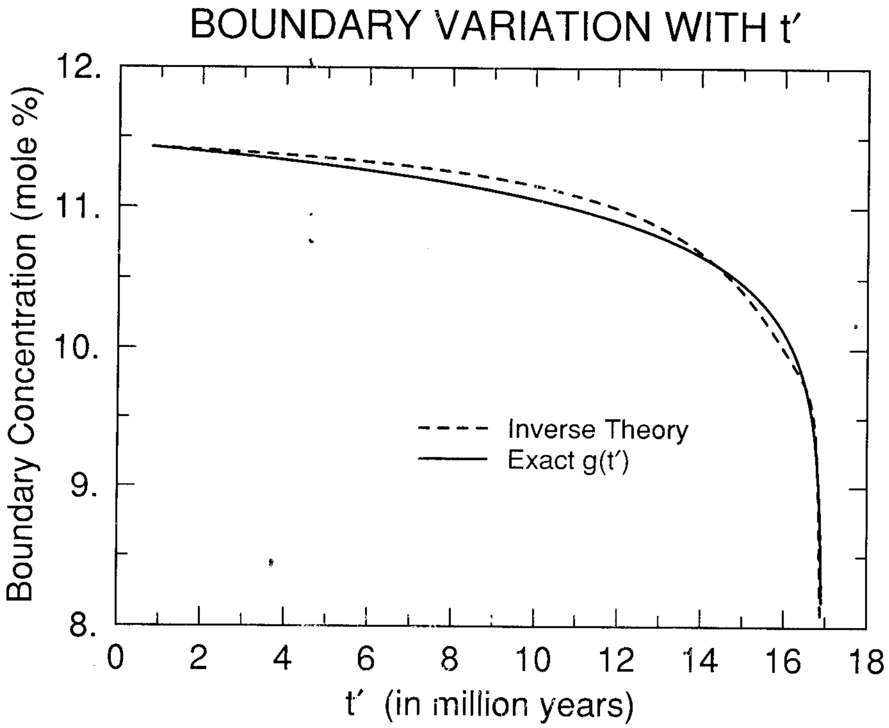

Fig. 21. Inversion of the perturbed zoning profile discussed in figure 14. In this case, random noise was added to the discretized zoning profile with a total error of 0.1 mole percent. The inversion uses the continuous functions given in eq (30) and minimization of the error using the NNLS method. Seven functions were used with A = 0 and B = 0.05, 0.1, 0.5, 1.0, 2.5, 4.0 and 6.0.

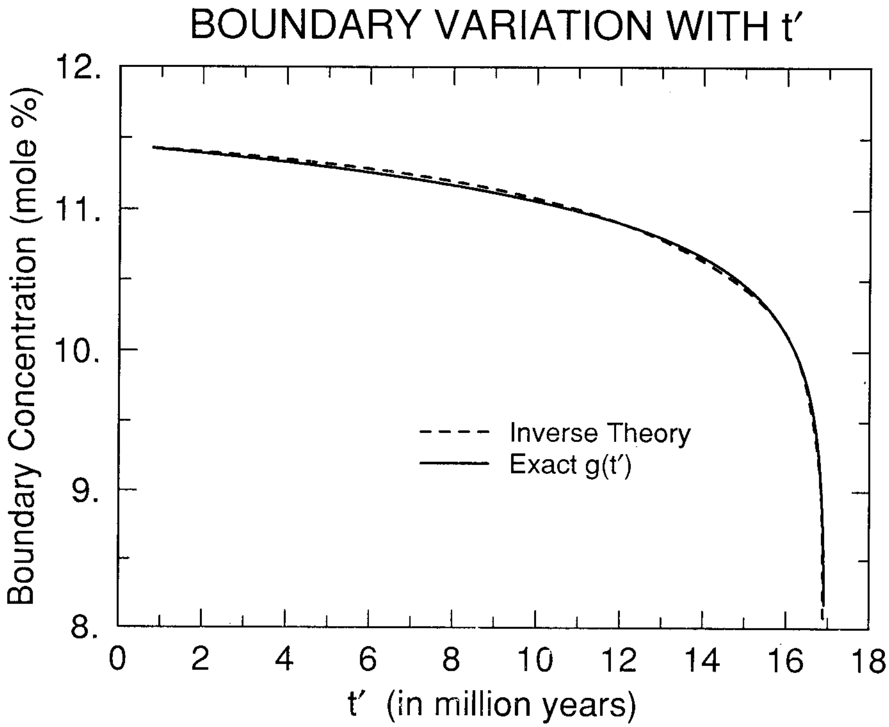

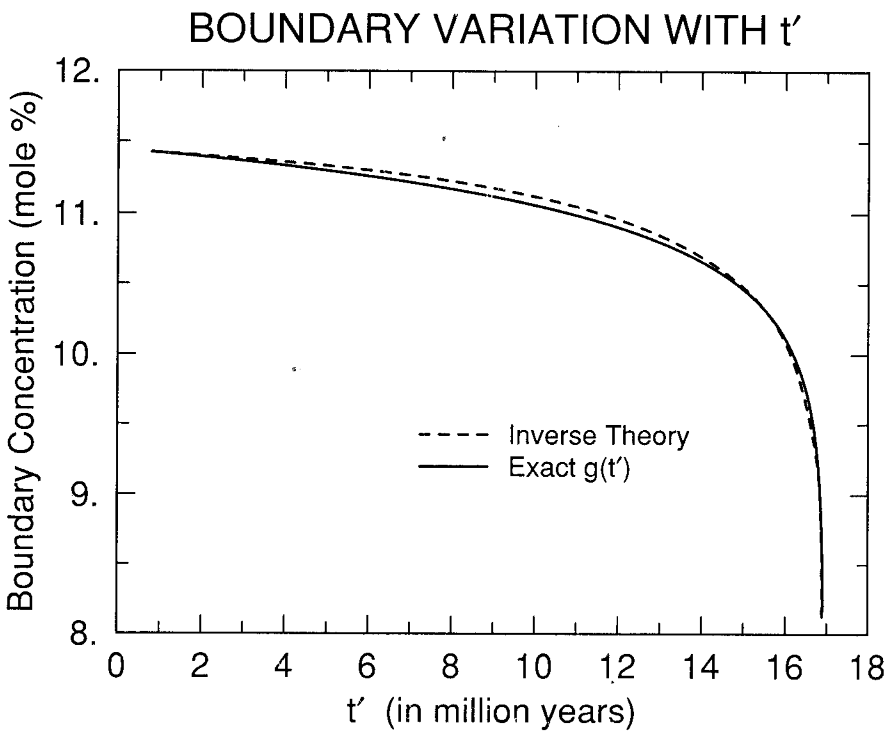

Fig. 22(A) Same as figure 20, but 3 new functions were added with B values of 0.02, 1.5, and 3.0 (that is, increased basis set).

(B) Same as figure 21 (that is, noisy profile), but 3 new functions were added with B values of 0.02, 1.5, and 3.0.

where the mineral with the slow diffusion coefficient has been identified as garnet in this case, and the equation is given for the boundary concentration of the other mineral, B, with the relatively fast diffusion coefficient. In eq (39), β stands for the rate of change of the cation exchange equilibrium constant, that is,

$$\beta \equiv -\frac{d\ln K_{eq}}{dt}$$

However, in the new treatment, β will be allowed to vary, because s is not constant and refers to the instantaneous value of dT/dt. From eq (2), we can rewrite this equation in a more convenient form as

$$\beta = -\frac{\Delta H_r}{RT^2}\frac{dT}{dt} \tag{40}$$

Combining eqs (39) and (40), using the Arrhenius equation for the diffusion coefficients and multiplying both sides by dt, it can be readily seen that $c_B(0, t)$ becomes only a function of temperature, T, that is,

$$dc_B(0, t) = -\frac{\dfrac{\Delta H_r}{RT^2}dT}{\sqrt{D_{Bo}/D_{gar,o}}\, exp\,(-(E_B - E_{gar})/2RT)\left(\dfrac{1}{c^I_{Mg,gar}} + \dfrac{1}{c^I_{Fe,gar}}\right) + \left(\dfrac{1}{c^I_{Mg,B}} + \dfrac{1}{c^I_{Fe,B}}\right)} \tag{41}$$

where E_i refers to the diffusion activation energy of mineral i, and D_0 is the diffusion preexponential factor. Eq (41) shows that $c_B(0, t)$ varies with t **only** through the time variation of T. Therefore, we can integrate this expression from the initial temperature, T_I, to temperature, T, to obtain the boundary concentration. This operation yields our expression for the boundary concentration:

$$c_B(0, t) = c_B(T(t)) = c^I_B - a\,ln\left[\frac{\left(1 + b\,exp\left(-\dfrac{E_{gar} - E_B}{2RT}\right)\right)}{\left(1 + b\,exp\left(-\dfrac{E_{gar} - E_B}{2RT_I}\right)\right)}\right] \tag{42}$$

where the constants a and b are given by:

$$a = \frac{2\Delta H_r c^I_{Mg,B} c^I_{Fe,B}}{(E_{gar} - E_B)c^{tot}_B}$$

$$b = \sqrt{\frac{D_{gar,o}}{D_{B,o}}\frac{c^I_{Mg,gar}c^I_{Fe,gar}c^{tot}_B}{c^I_{Mg,B}c^I_{Fe,B}c^{tot}_{gar}}}$$

and $c_i^{tot} = c_{Mg}^I + c_{Fe}^I$ for mineral i. The one caveat in using eq (42) is that if the rate of change of temperature changes sign (for example, from heating to cooling), the value of c_B at the peak of heating or cooling becomes the new c^I, and the value of T at the peak of heating or cooling (that is, where the rate goes to zero) becomes the new T_I in the equations. In this manner, eq (42) can handle situations in which the temperature is undergoing both heating as well as cooling. We will see an application of this equation to the case of the heating and cooling thermal history of a dike.

Once we obtain the boundary concentration, $c_B(0, t)$, for the slower varying boundary, we can use the exact relation to obtain the boundary concentration for garnet (which is the more crucial boundary). Thus, using eqs (1) and (2):

$$c_{gar}(0, t) = \frac{c_B(0, t)c_{gar}^{tot}K_{eq}(T(t))}{c_B^{tot} + (K_{eq}(T(t)) - 1)c_B(0, t)} \tag{43}$$

where $c_B(0, t)$ is given by eq (42).

Eqs (42) and (43) yield an analytical formula for $c_{gar}(0, t)$ as a function of T. By solving the equation (for example, by Newton-Raphson methods), this formula can also yield T as a function of $c_{gar}(0, t)$, which is the relation we use in the next section.

It is important to test these equations for the boundary concentration under complex conditions. We ran two tests: one involved the thermal history of a dike intrusive, and the other the earlier model of regional metamorphism arising from uplift and erosion. Figure 23 illustrates the close agreement between calculated and exact boundary concentrations for the case of a dike with $T_0 = 1175°C$, $T_R = 300°C$, a half-width of 800 m, and a 210 μ sized garnet 25 m from the contact. The pressure was assumed to be 1 kb, and the Ferry and Spear (1978) K_D data and the Cygan and Lasaga (1985) garnet diffusion data were used. Clearly, the scheme discussed above works very well for the dike thermal history.

Figure 24 exhibits the same comparison for the regional model in which $z_M = 25$ km, $T_m = 650°C$, $v_z = 0.3$ cm/yr, and the garnet is 350 μ long. Once more the agreement is fairly good even though the pressure variation during the uplift history added to the error.

These calculations show that, while the model leading up to eqn (43) is not exact, the errors are small enough that the equation can serve as a useful start into the tomographic inversions.

From g(t′) to T(t).—Having obtained g(t′) and with a relation between T and $c_{boundary}$, all that is left is to combine the two results to obtain the thermal history. In fact, from $T(c_{boundary})$ and g(t′) (which is $c_{boundary}(t')$), it is easy to obtain T(t′). As an example of the reliability of this step, figure 25 compares the calculated T(t′) with the exact curve for the case of the dike intrusion model discussed at the end of the last section. This figure shows

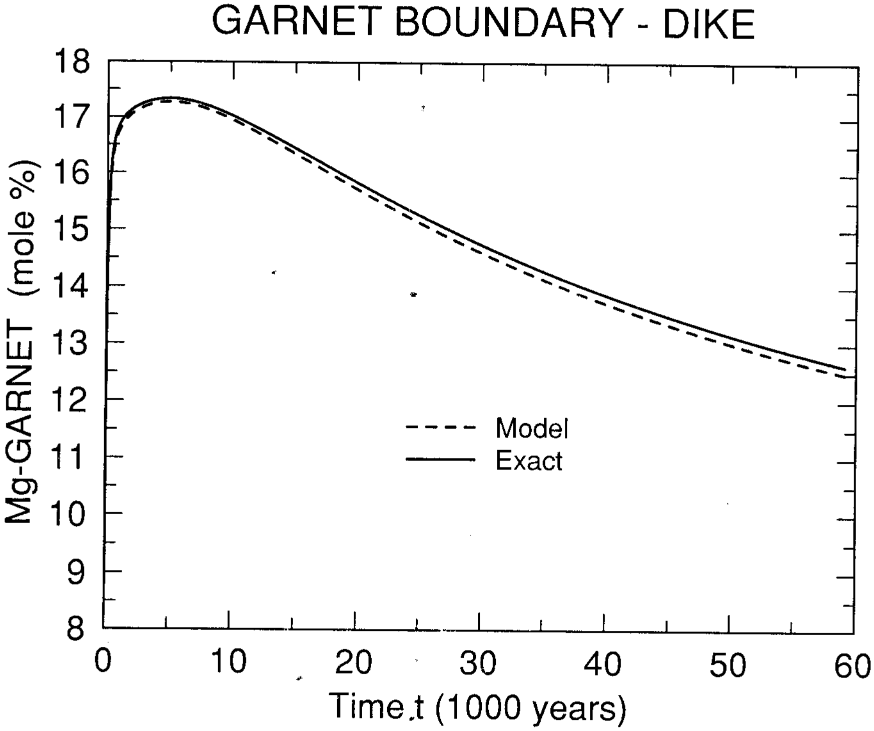

Fig. 23. Comparison of calculated (eq 36) and exact boundary concentrations as a function of time for the case of the contact metamorphic model discussed in figures 9 and 10.

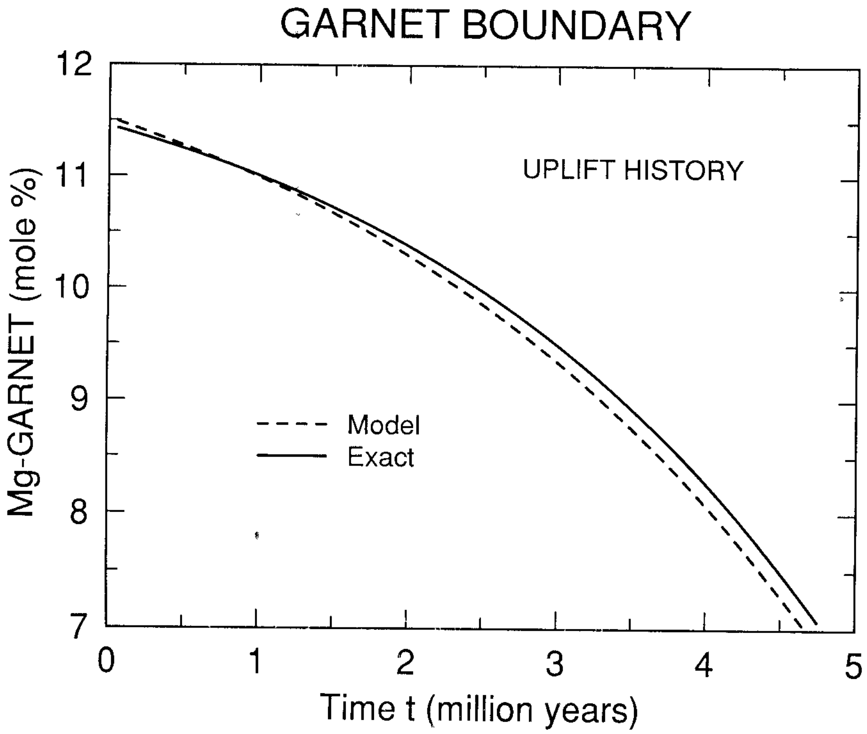

Fig. 24. Comparison of calculated and exact boundary concentrations for the same regional metamorphic history used in figure 19. The garnet size is now 350 microns.

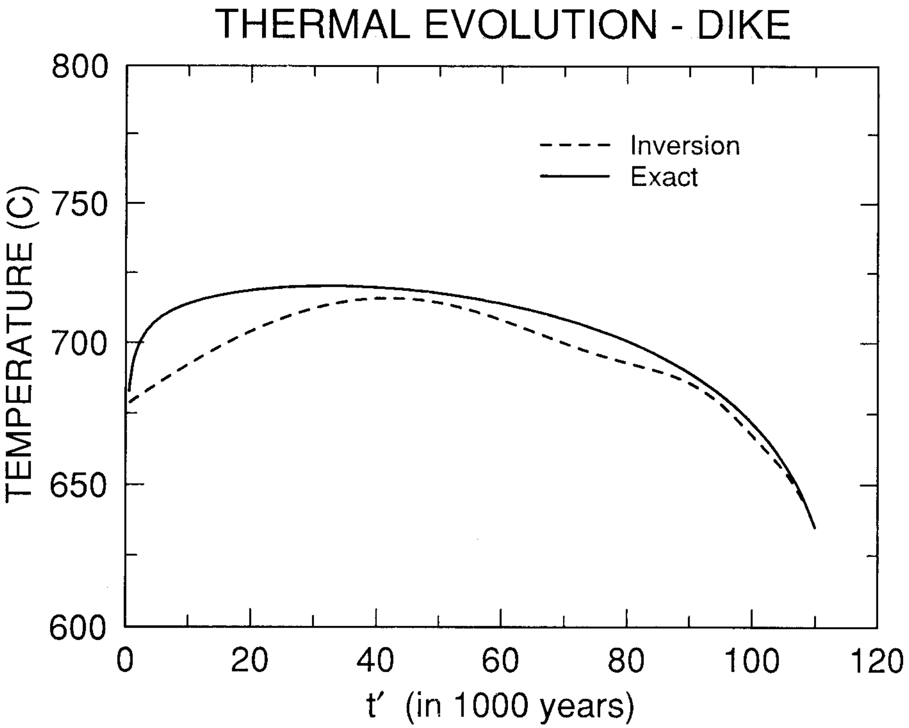

Fig. 25. Calculated temperature variation as a function of t′ for the contact metamorphic case used in figures 9 and 10.

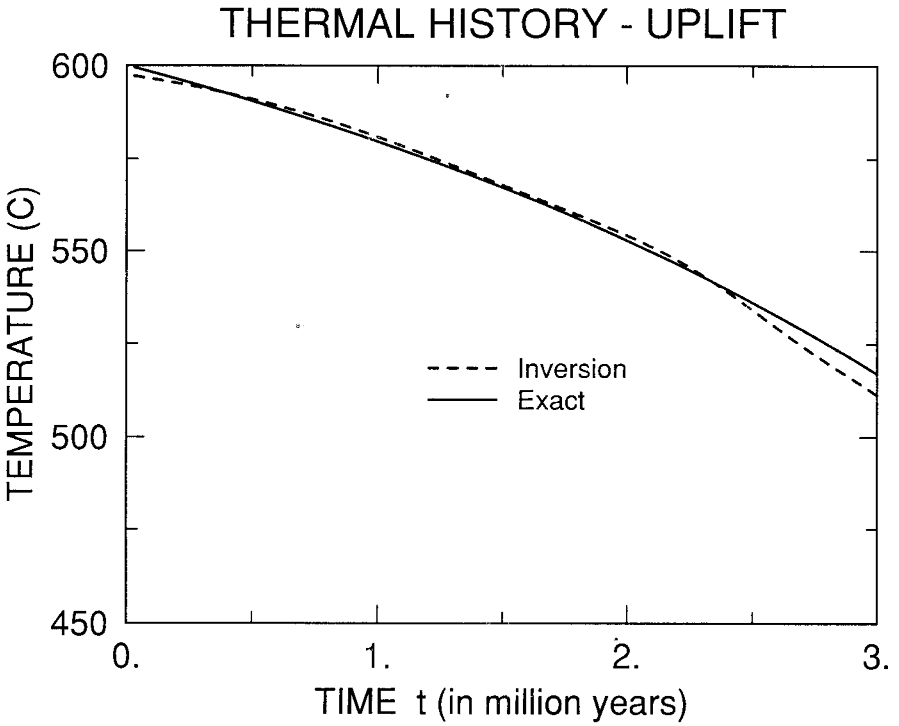

Fig. 26. Full inversion of the thermal history for a regional metamorphic garnet compared with the "exact" history. Note that these inversions use typical profiles, that is, a discrete set of data on concentration as a function of distance from the rim of the garnet. The data are spaced several microns apart, and "noise" is added!

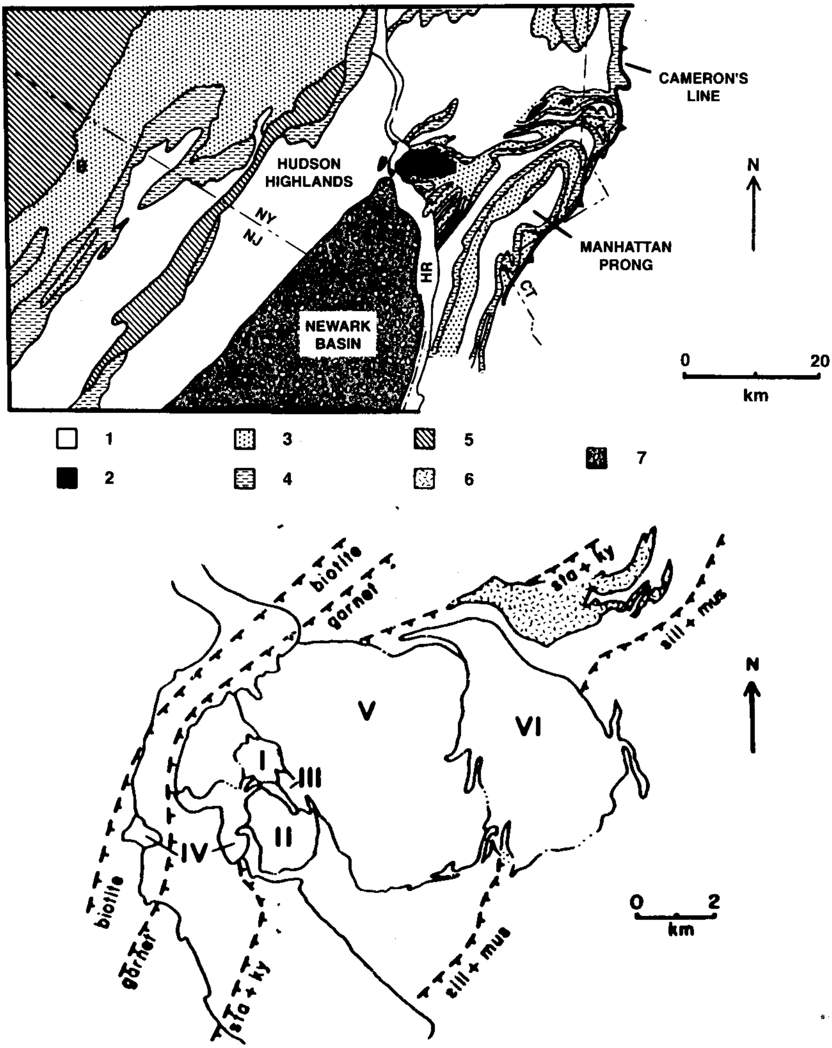

Fig. 27(A) Location of the Cortlandt Complex in New York (shown in dark black near the middle) (from Waldron, ms).

(B) Details of the multiple intrusive events making up the Cortlandt Complex. The Complex is a composite, mafic to ultramafic body located in Westchester County, New York. It intrudes across a steeply-dipping Barrovian regional metamorphic sequence of mineral assemblages, *which were* formed as part of the Taconic orogeny (Waldron, ms).

that the relation can be used not only for cooling events but also for thermal histories involving both heating and cooling events. To proceed further it is useful to note that:

$$\frac{dT}{dt} = \frac{dT}{dt'}\frac{dt'}{dt}$$

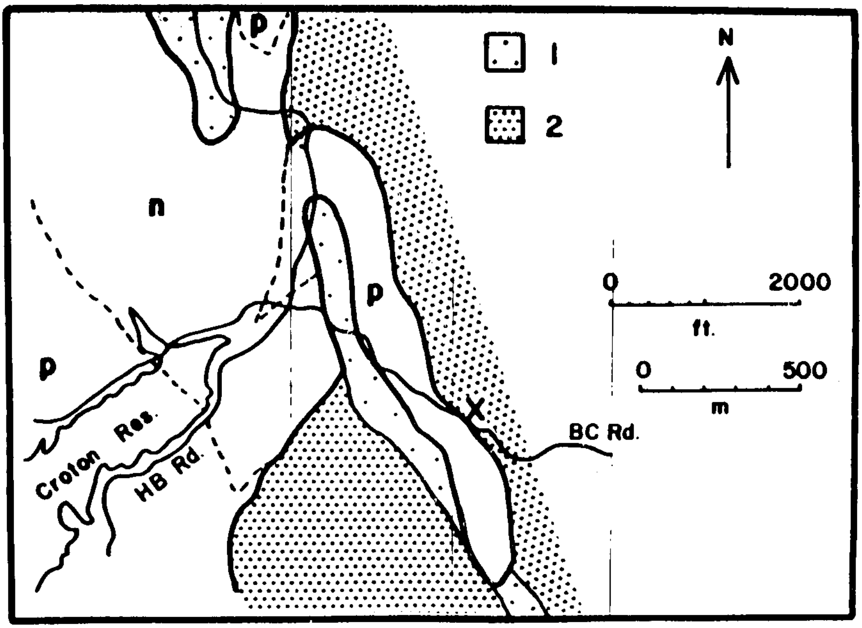

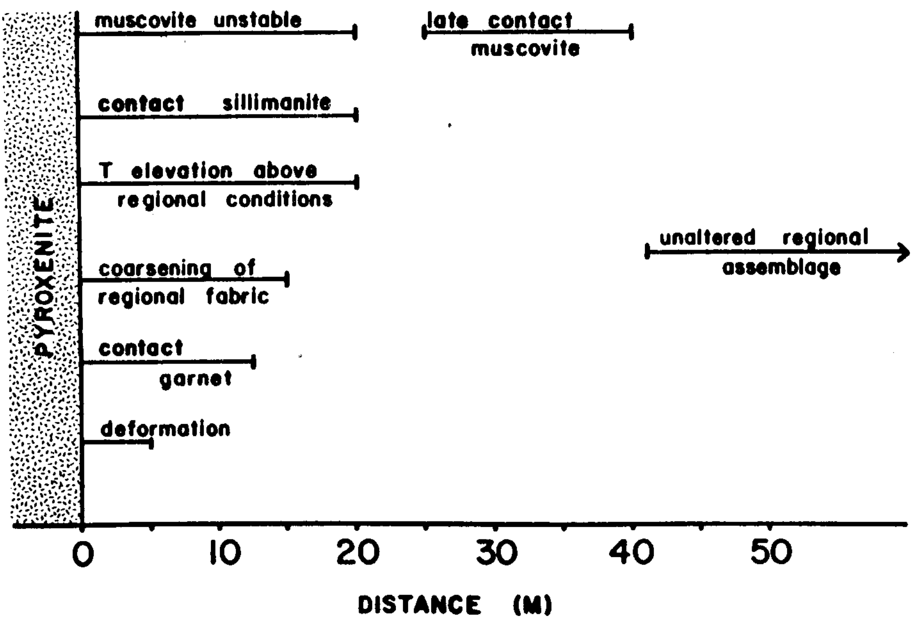

Fig. 27(C) Blow up of the Cortlandt Complex showing the location of our samples (marked by X). p—pyroxenite, n—norite. (from Waldron, ms)

(D) Contact aureole around the pyroxenite intrusion in the Cortlandt Complex (from Waldron, ms).

Using eq (12) to evaluate dt′/dt results in

$$\frac{dT}{dt} = \frac{dT}{dt'} \, exp\left[-\frac{E_a}{R}\left(\frac{1}{T(t')} - \frac{1}{T_0}\right)\right] \tag{44}$$

If T(t′) is known, then eq (44) can be used to integrate the full thermal history, T(t). Typically, one begins with an initial temperature, T_{init} (which does not have to be equal to T_0). At this point, dT/dt, is evaluated using eq (44). A new temperature at Δt is obtained:

$$T(\Delta t) = T_{init} + \frac{dT}{dt}\,\Delta t$$

Using T_{init} and T(Δt), a new value of t′ at Δt is computed by integrating eq (12) and assuming a constant dT/dt in this small time interval. Using the new value of t′, dT/dt′ is obtained from T(t′), and another dT/dt is computed. This process is repeated to obtain T at subsequent time intervals until the entire T(t) curve is generated. Figure 26 illustrates the calculation for the regional metamorphism model (T_m = 600°C, v_z = 3 mm/yr, z_m = 25 km) discussed earlier. The comparison with the exact thermal history is fairly good.

At this point, all the necessary tools are in place for applying the techniques developed here to extract T(t) in a wide variety of geological situations. The next section illustrates a contact metamorphic example.

Geological example: Cortlandt Complex, New York.—As an initial application of the techniques outlined here, a systematic study of the zoning profiles in the aureole of the Cortlandt Complex, southeastern New York was undertaken. The Cortlandt Complex (fig. 27) is a composite, mafic to ultramafic body located in Westchester County, New York, about 40 km north of New York city (Waldron, ms). The composite plutons intruded across a steeply-dipping Barrovian regional metamorphic sequence of mineral assemblages, formed as part of the Taconic orogeny. The contact metamorphic event is believed to have occurred in the waning stages of the regional metamorphism. Figure 27B shows the location of the samples analyzed in this study. Figure 27 shows the extent of the contact aureole. Various garnets at different distances from the contact with the pyroxenite were microprobed.

A very important consideration in developing the geospeedometry technique is the degree to which various garnets exhibit similar zoning profiles. For example, if growth has ceased and several garnets have experienced the same thermal history and are texturally similar (that is, have adjacent biotites or cordierites et cetera), then their zoning profiles should be similar. Likewise, if no growth has occurred, the zoning between a garnet and a biotite at its rim should agree with the zoning between that garnet and a biotite inclusion (assuming that the biotite inclusion is not too small, for example, greater than the distance of the zoning profiles in the garnet). Figure 28 gives four scans across different segments of a biotite inclusion in a garnet 25 m from the contact and exhibits the close similarity in the results. Figure 29 compares the zoning

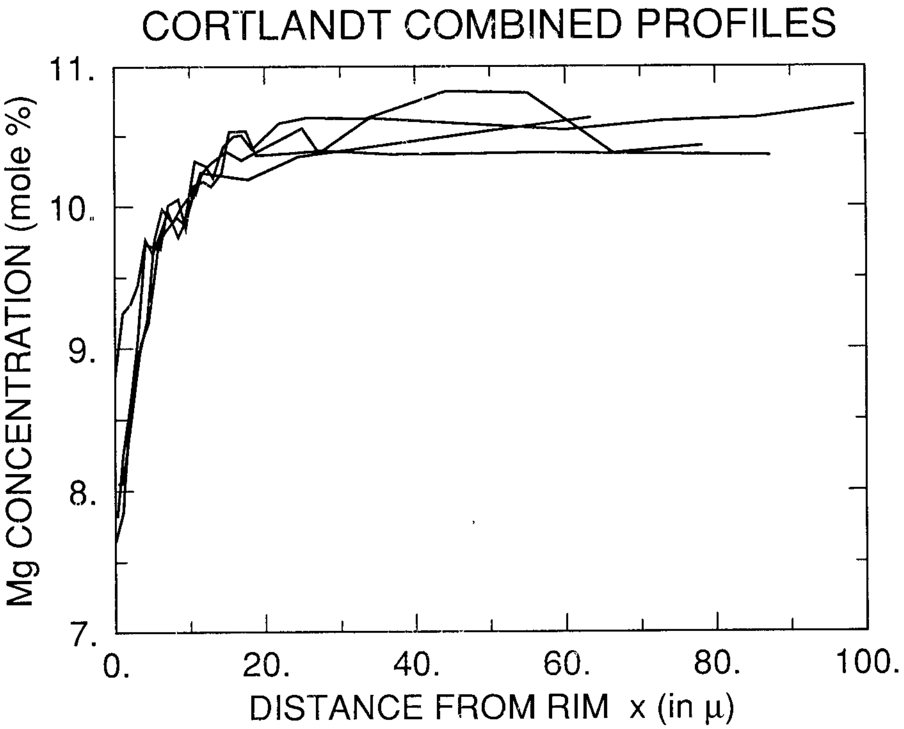

Fig. 28. Magnesium zoning profiles in a garnet 25 m from the contact. The garnet is in contact with a biotitle inclusion.

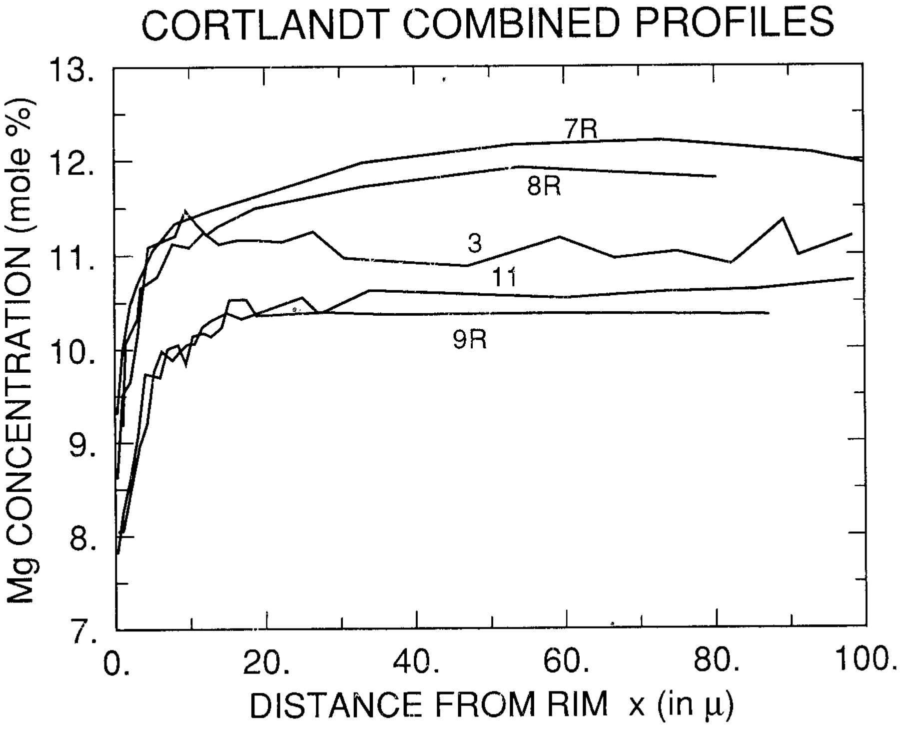

Fig. 29. Comparison of magnesium zoning profiles in garnets 7 m (8R and 7R) and 25 m (9R and 11) from the contact and in contact with a biotite inclusion. Scan 3 is a garnet 25 meters from the contact adjacent to a biotite grain.

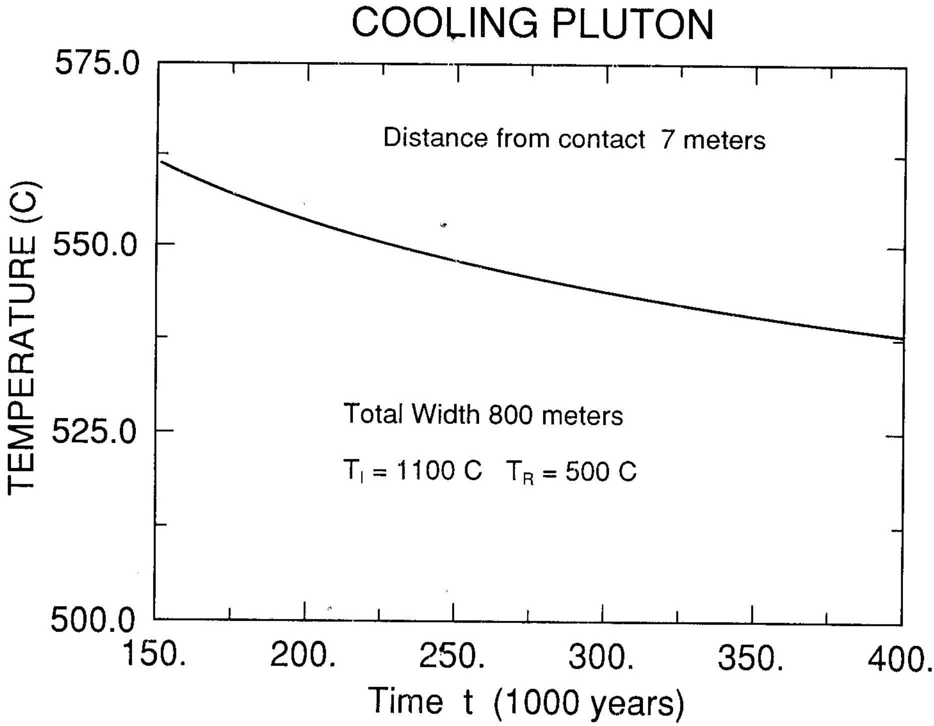

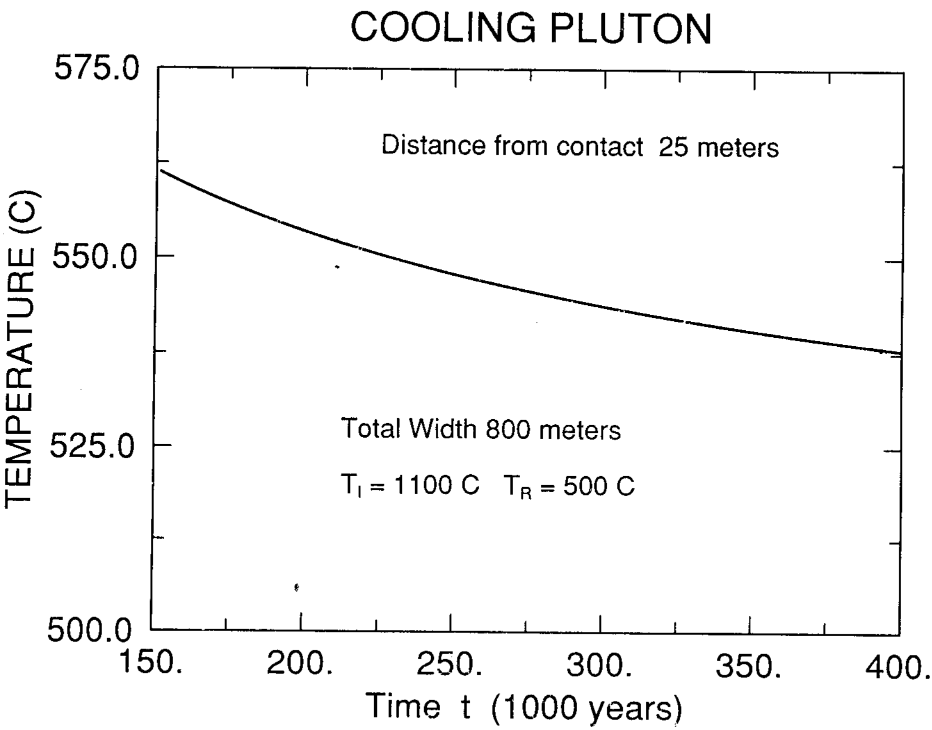

Fig. 30(A) Thermal history calculated for an intrusion with a half-width of 500 m and T_i = 1100°C and T_r = 500°C. The distance is 7 m from the contact. (B) Same as (A) but at a distance of 25 m from the contact.

profiles between garnet and biotite inclusions 7 and 25 m from the contact. Figure 29 also includes data for garnet in contact with biotite at its rim (7 m from the contact—scan 3). In the case of a large intrusion (for example, 500 m in width or greater), the thermal history experienced by a 7 or 25 m garnet should be the same (for example, see fig. 30). Therefore, the profiles in all the 7 or 25 m garnets should be similar. The profiles in figure 29 are very similar indeed. In fact, if the three top profiles are simply lowered, the agreement in the **shape** of the profiles is verified as shown in figure 31. The profiles exhibited in figures 29 and 31 demonstrate two points: (1) the garnet profiles are consistent with a thermal history for the cooling of a large intrusion (fig. 25), and (2) the similarity in the zoning profiles of several garnets forms the basis for the systematic application of inverse theory.

Of course, the purpose of developing the techniques described in this paper is to extract quite detailed histories from the zoning profiles. The continuous functions discussed earlier were used to invert the garnet profile (scan 9R), and the results are shown in figure 32. Note that the calculated thermal history has the correct "shape" for the cooling of an

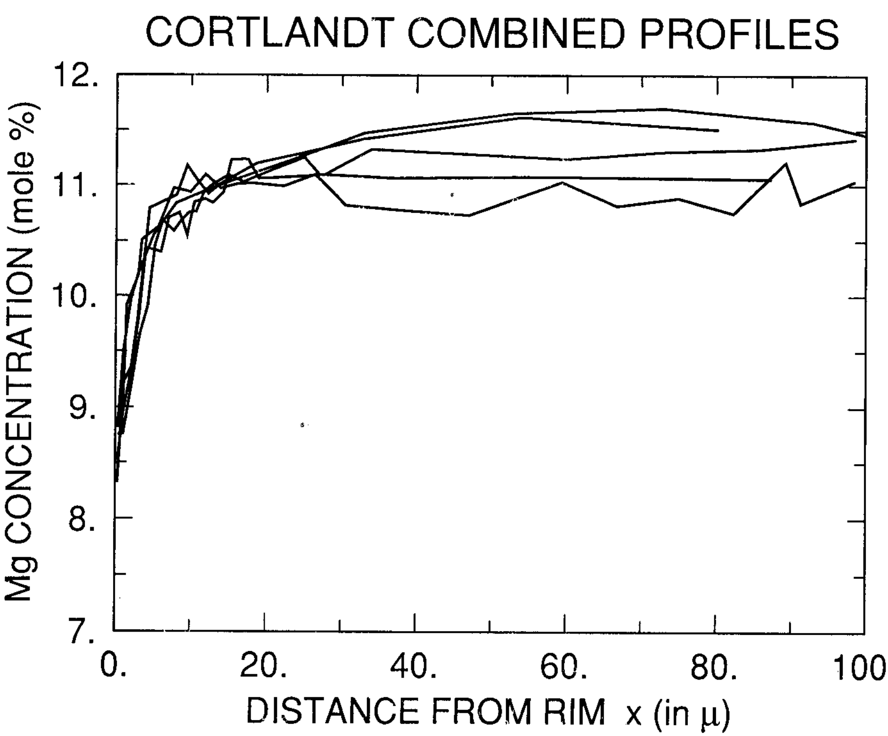

Fig. 31. Superposition of the profiles in figure 29 by shifting the vertical positioning.

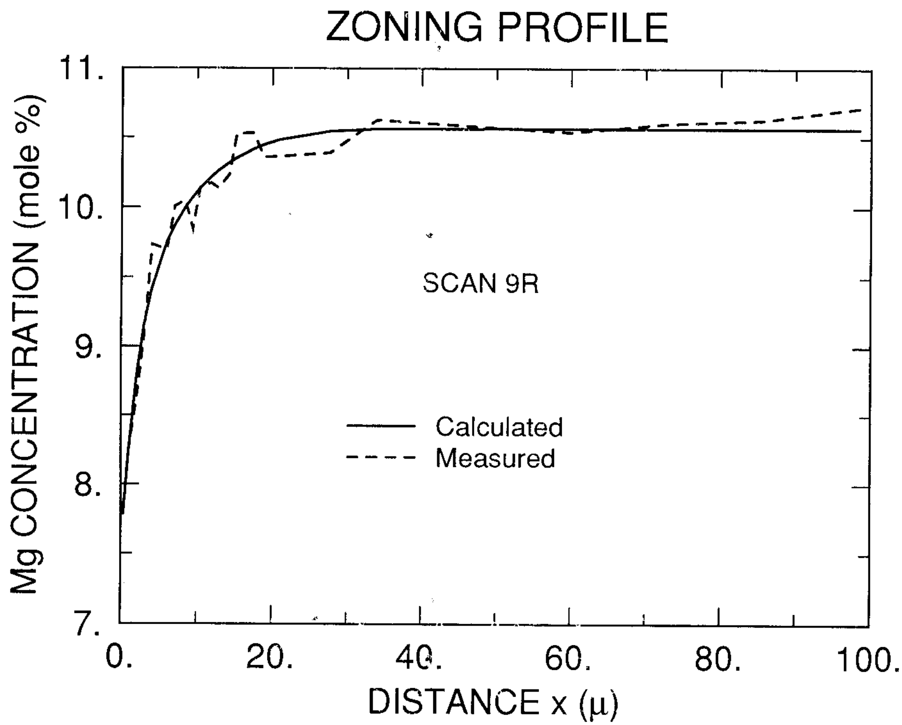

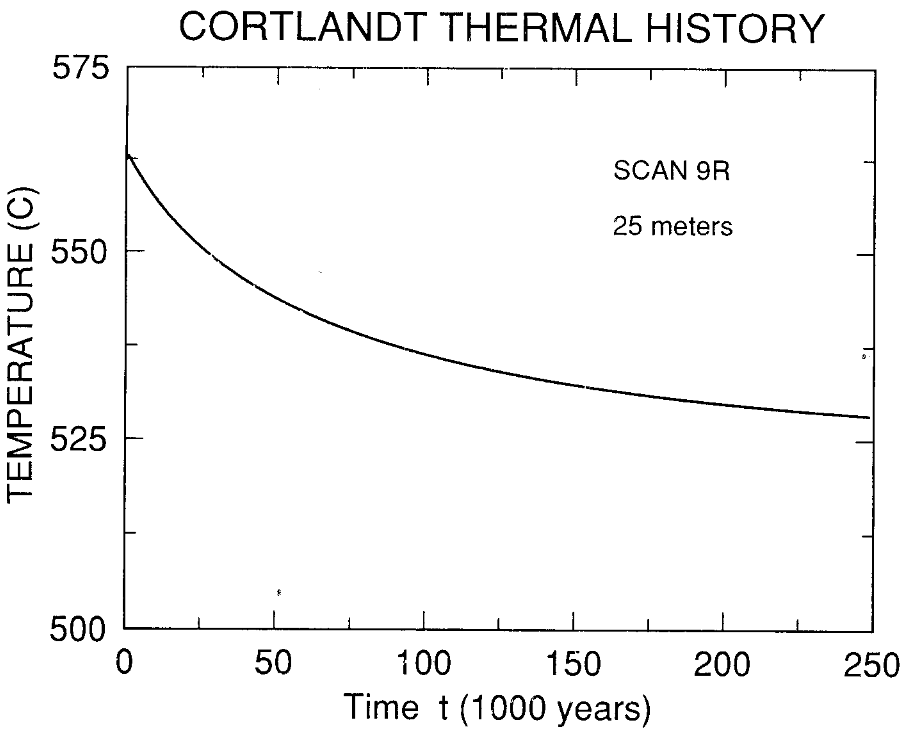

Fig. 32(A) Inversion of the zoning profile 9R in garnet 25 m from the contact. The smooth curve is the result of the "inversion." (B) Temperature-time history predicted from the inversion.

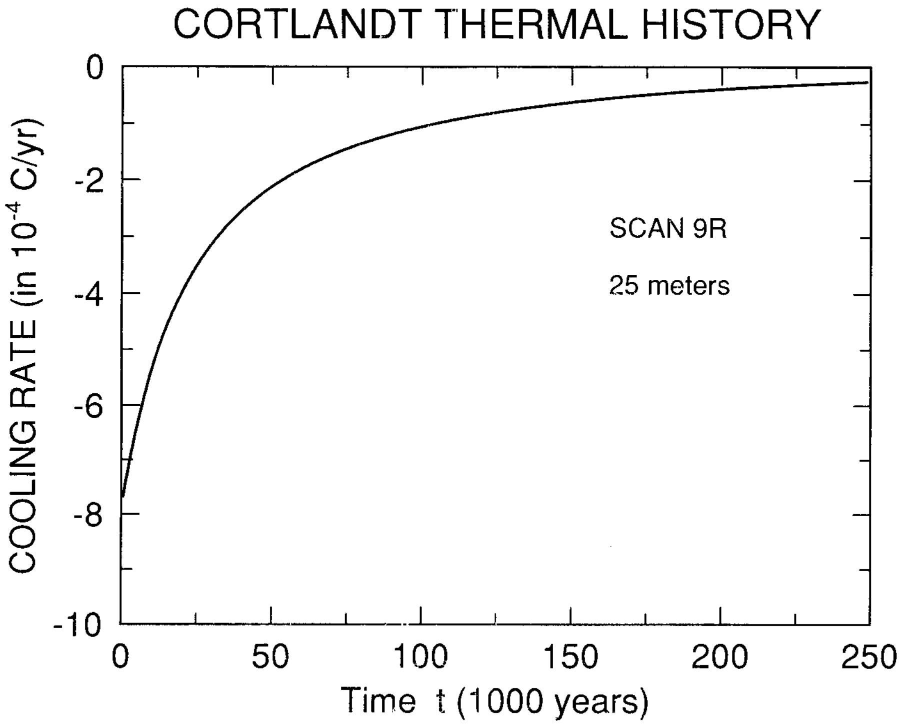

Fig. 32(C) Cooling rate as a function of time predicted from the inversion.

intrusion, that is, a fast initial cooling rate decays to slower cooling rates with time. Note that the technique is not limited to a single cooling rate as in simpler models. A similar inversion using the data from 7 m from the contact (scan 8R) is shown in figure 33. As discussed above, the two thermal histories agree well with each other. The calculated histories are consistent with predicted conductive cooling histories of plutons. For example, figure 34 exhibits the conductive cooling history of a rock 25 m from an 800 m wide dike (T_I = 1175°C and T_{rock} = 500°C). As expected from the forward model results discussed earlier, the inverse method accurately computes the details of the thermal history. Note that the simple model assumed in figure 34 is not to be taken as the "answer" to the problem, but rather the simple results merely show that the more general answer given by the inversion makes geological sense.

A garnet that shows a growth outer rim at a distance of 2.5 m from the contact exhibits quite a different zoning profile (fig. 35). Inversion of this zoning profile yields quite a different thermal history, which is not consistent with cooling of the pluton (fig. 36). In this case, the **growth** of a garnet has played a key role in the observed zoning profile. This growth

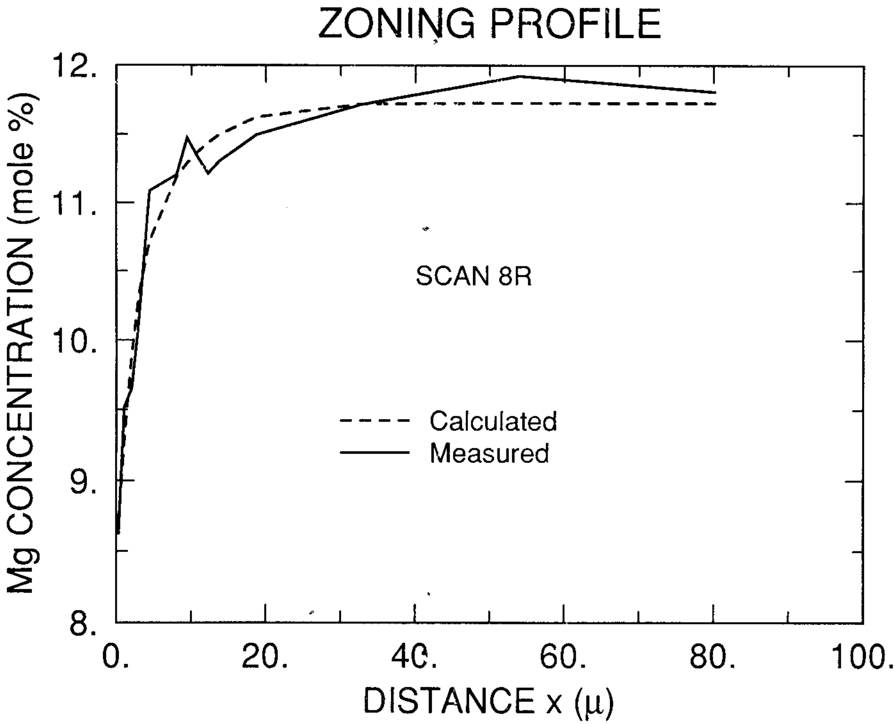

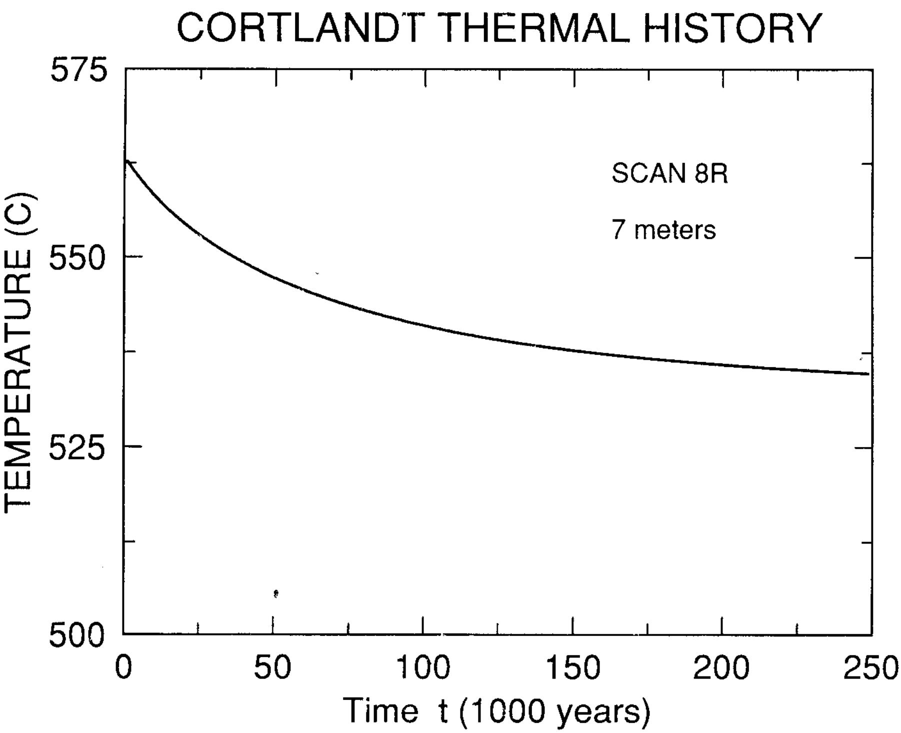

Fig. 33(A) Inversion of the zoning profile 8R in garnet 7 m from the contact. The smooth curve is the result of the "inversion." (B) Temperature-time history predicted from the inversion.

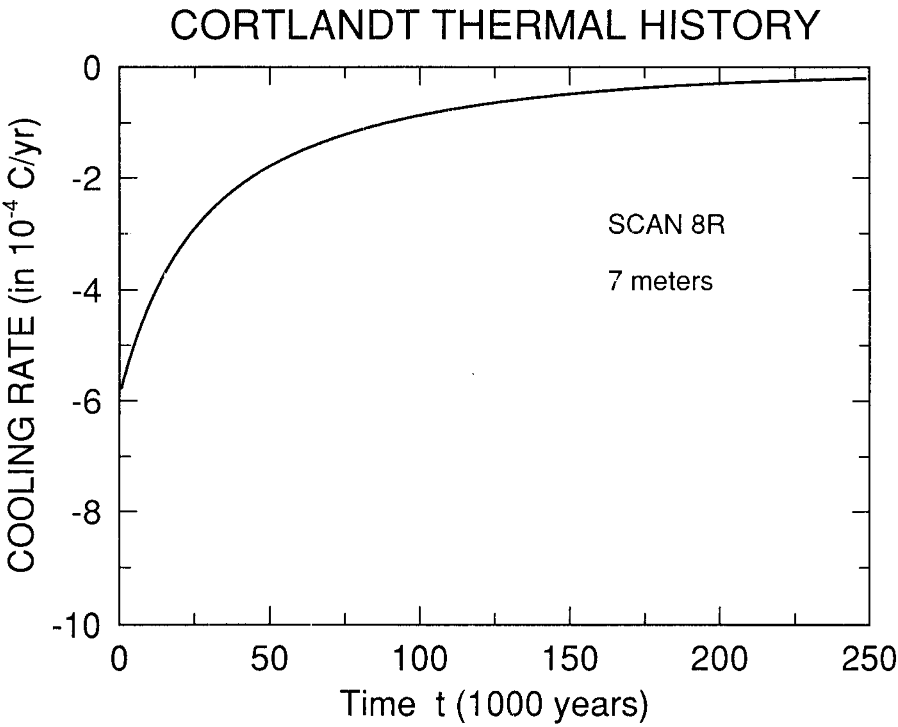

Fig. 33(C) Cooling rate as a function of time predicted from the inversion.

must have occurred during or after the high temperature part of the cooling thereby obscuring the diffusion profiles.

Note that the inclusions in the garnets at 7 and 25 m away from the contact would have had to record the heating part of the thermal history, if the garnet-biotite pairs were present during the heating. The fact that the zoning profiles between garnet and inclusions only "see" the cooling of the pluton strongly suggests that these garnets also grew during the heating event. This result is different from the conclusions in Waldron (ms). It can be shown that for a wide range of diffusion coefficients (several orders of magnitude) the response of a garnet-biotite contact pair to a heating and cooling event would lead to pronounced maxima in the final quenched zoning profiles. For example, in the case of an 800 m intrusion, the calculated final zoning profile has been shown in figure 10.

CONCLUSIONS

The quantitative treatment of zoning data in minerals can unlock the important tectonic and thermal history data contained in the zoning. This paper extends previous treatments of zoning by attacking the

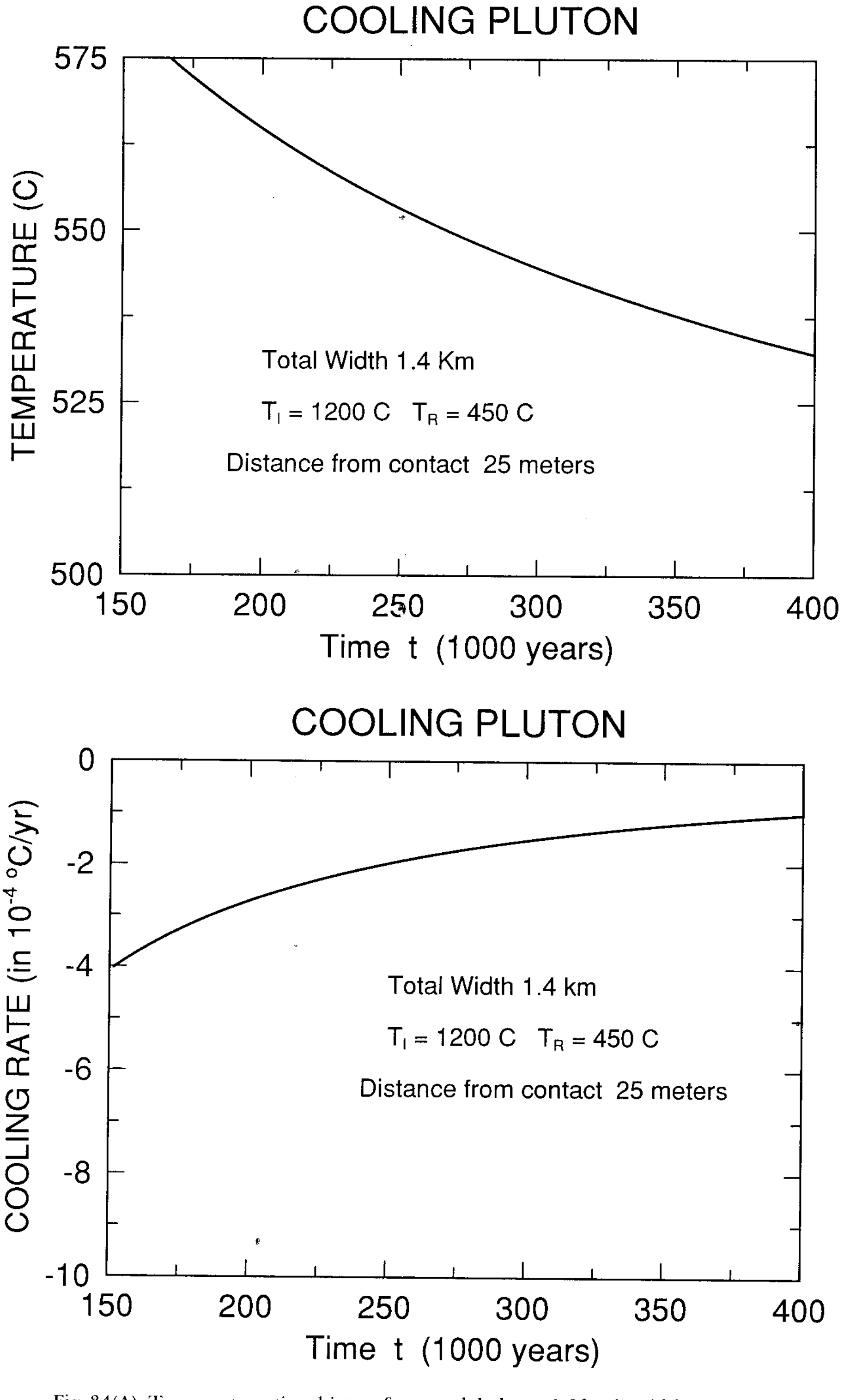

Fig. 34(A) Temperature-time history for a model pluton 1.6 km in width (800 m in half width) at a distance of 25 m from the contact. (B) Cooling rate history for the same site. Compare this figure with the inversion of the garnet data in figures 32 and 33.

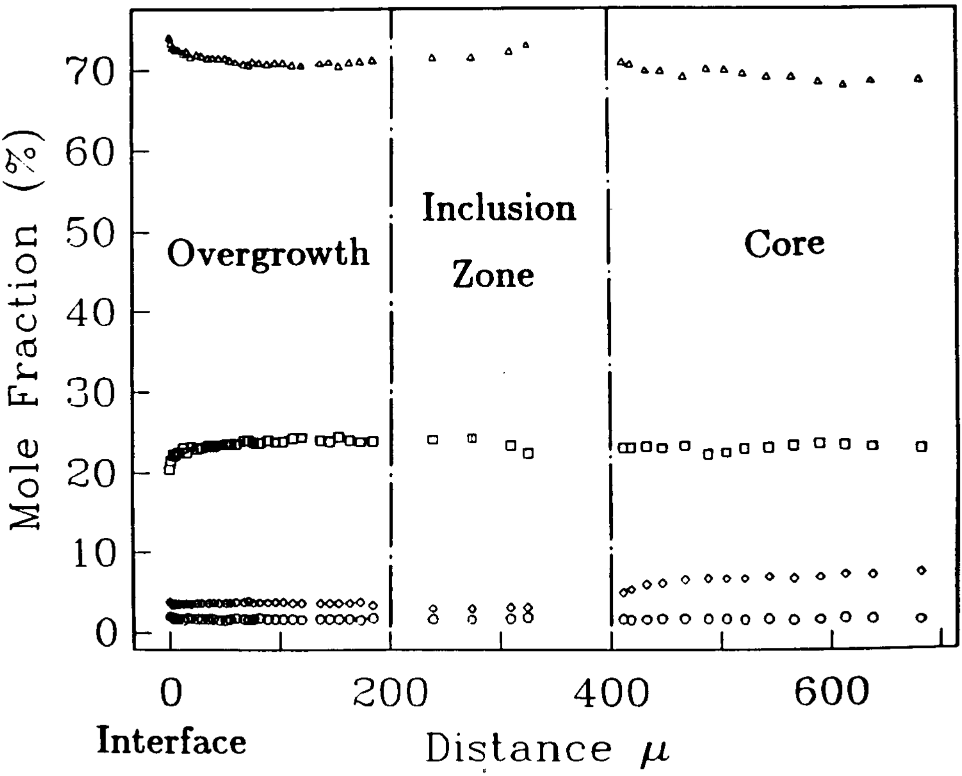

Fig. 35. Zoning profile of the garnet exhibiting complex growth history at a distance of 2.5 m from the contact.

quantification using all the tools available from inverse theory. Simple models (using contour plots based on few parameters) illustrate the sensitivity of the zoning profiles to the history of a rock. Full inverse theory calculations then illustrated the ability to invert the history from zoning profiles by comparing the inversion with forward models. A very important result showed that these inversions did **not** require a simple model such as constant "cooling rate" but could handle and predict complex thermal histories. The results presented in this paper underscore the power of using the available mineral zoning data in a detailed kinetic model. The recording of kinetic P-T paths (that is, with time added!) will be readable not only for garnets but for any assemblages where diffusion is a strong function of temperature (which is a general phenomenon). For example, it should work for mineral assemblages such as sphalerite-pyrrhotite-pyrite in the sphalerite geobarometer. The feasibility of the method has been shown not only for a variety of forward models but also for a particular field example involving the Cortlandt

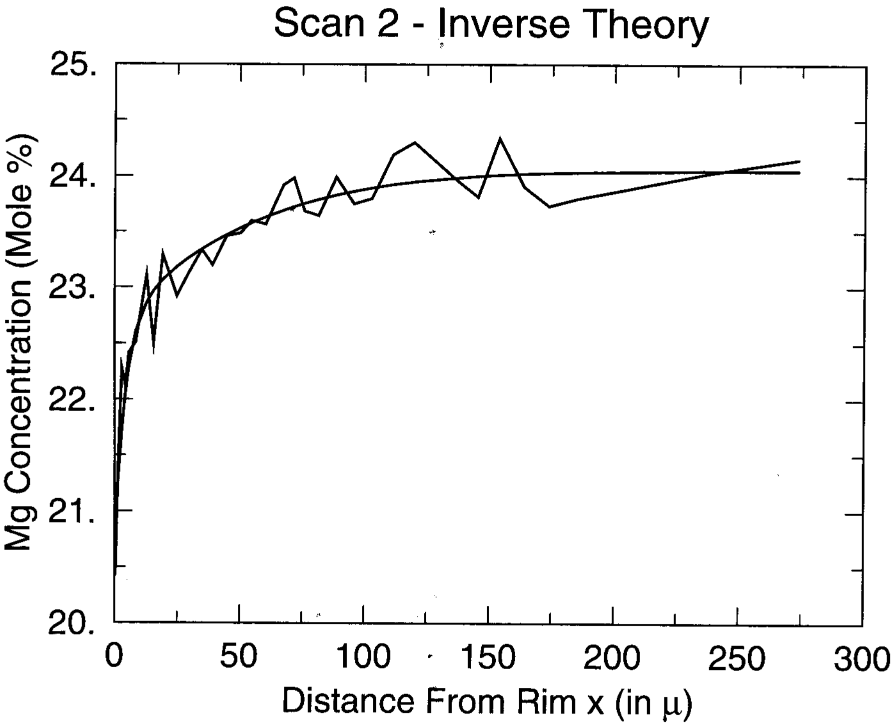

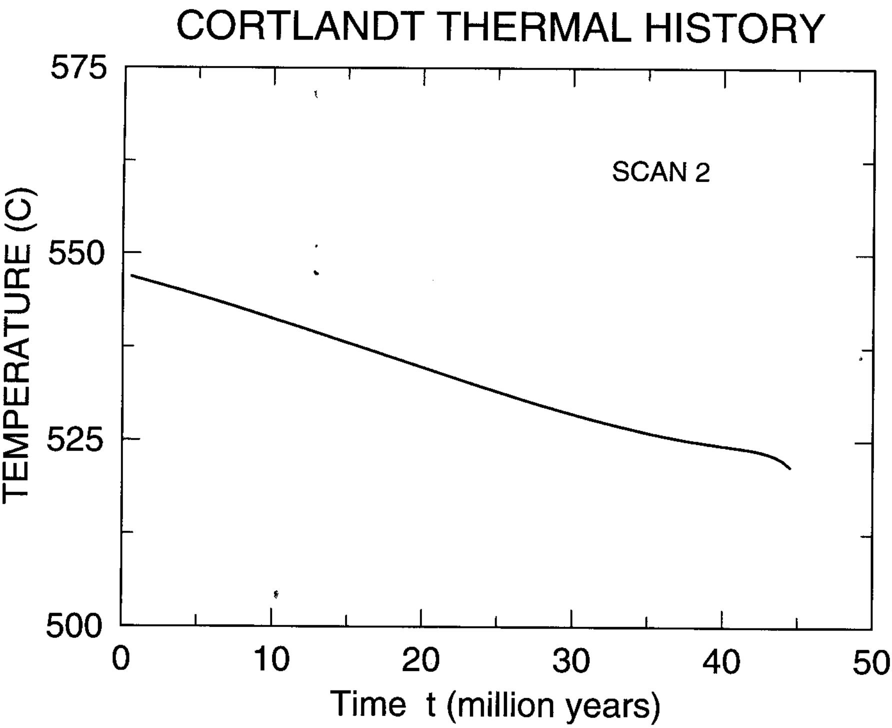

Fig. 36. Inversion of the edge zoning profile for the garnet in figure 35.

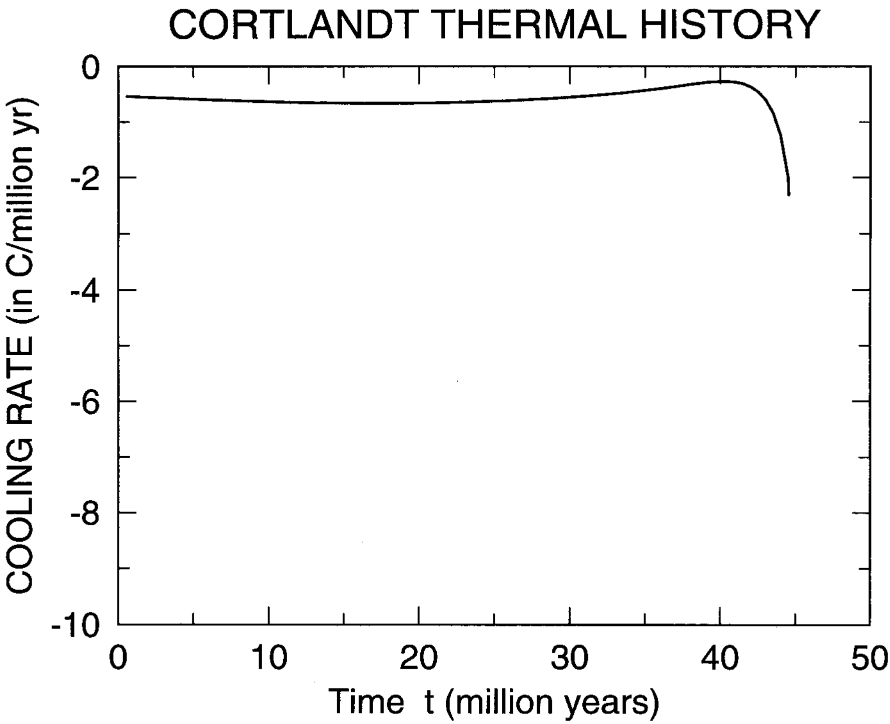

Fig. 36. (continued)

Complex aureole in New York. Future work will continue to apply the powerful techniques developed here to a variety of tectonic settings, especially regional metamorphic cases and their concomitant tectonic implications.

ACKNOWLEDGMENTS

The authors would like to acknowledge gratefully financial support through the National Science Foundation (NSF EAR 9017976, EAR 9219770, EAR 89117056, EAR 9316608) and the Department of Energy (DE-FG02-90-ER 14153). The senior author would also like to acknowledge the help of a Fairchild Fellowship at the California Institute of Technology and a Humboldt Fellowship at Bayreuth and Tubingen, Germany. The careful reviews by Frank Spear, Phil England, and Sumit Chakraborty were very helpful to improve the final paper.

REFERENCES

Berg, J. H., and Docka, J. A., 1983, Geothermometry in the Kiglapait contact aureole, Labrador: American Journal of Science, v. 283, p. 441–434.

Bergman, S., 1992, P-T paths in the Handol area, central Scandinavia: record of Caledonian accretion of outboard rocks to the Baltoscandian margin: Journal of Metamorphic Geology, v. 10, p. 265–281.

Chamberlain, C. P. and England, P. C., 1985, the Acadian thermal history of the Merrimack synclinorium in New Hampshire: Journal of Geology, v. 93, p. 593–602.
Clarke, G. L., and Powell, R., 1991, Proterozoic granulite-facies metamorphism in the southeastern Reynolds Range, central Australia: Geological context, P-T path and overprinting relationships: Journal of Metamorphic Geology, v. 9, p. 267–281.
Cygan, R. T., and Lasaga, A. C., 1982, Crystal Growth and the Formation of Chemical Zoning in Garnets: Contributions to Mineralogy and Petrology, v. 79, p. 187–200.
——— 1985, Self-diffusion of magnesium in garnet at 750 to 900°C. American Journal of Science. v. 285, p. 328–350.
Dempster, T. J., 1985, Garnet zoning and metamorphism of the Barrovian type area, Scotland: Contributions to Mineralogy and Petrology, v. 89, p. 30–38.
Docka, J. A., Berg, J. H., and Klewin, K. H., 1986, Geothermometry in the Kiglapait aureole. II. Evaluation of exchange thermometry in a well-constrained thermal setting: Journal of Petrology, v. 27, p. 605–626.
Elphick, S. C., Ganguly, J., and Loomis, T. P., 1985, Experimental determination of cation diffusivities in aluminosilicate garnets. I. Experimental methods and interdiffusion data: Contributions to Mineralogy and Petrology, v. 90, p. 36–44.
Essene, E. J., 1982, Geologic thermometry and barometry, *in* Ferry, J. M., editor, Characterization of Metamorphism Through Mineral Equilibria: Mineralogical Society of America, Reviews in Mineralogy, v. 10, p. 153–206.
Ferry, J. M., and Spear, F. S., 1978, Experimental calibration of the partitioning of Fe and Mc between biotite and garnet: Contributions to Mineralogy and Petrology, v. 66, p. 113–117.
Florence, F. P. and Spear, F. S., 1991, Effects of diffusional modification of garnet growth zoning on P-T path calculations: Contributions to Mineralogy and Petrology, v. 107, p. 487–500.
Goffe, B., Michard, A., Kienast, J. R., and Olivier, Le M. K., 1988, A case of obduction-related high-pressure, low-temperature metamorphism in upper crustal nappes, Arabian continental margin, Oman: P-T paths and kinematic interpretation: Tectonophysics, v. 151, p. 363—386.
Hansen, V. L., 1992, P-T evolution of the Teslin suture zone and Cassiar tectonites, Yukon, Canada: evidence for A- and B-type subduction: Journal of Metamorphic Geology, v. 10, p. 239–263.
Harrison, T. M., Lovera, O. M., and Heizler, M. T., 1991, $^{40}Ar/^{39}Ar$ results for alkali feldspars containing diffusion domains with differing activation energy: Geochimica et Cosmochimica Acta, v. 55, p. 1435–1448.
Jiang, J. and Lasaga A. C., 1990, The effect of post-growth thermal events on growth-zoned garnet: Implications for metamorphic P-T history calculations: Contributions to Mineralogy and Petrology, v. 105, p. 454–459.
Lamb, W. M., Brown, P. E., and Valley, J. M., 1991, Fluid inclusions in Adirondack granulites: Implications for the retrograde P-T path: Contributions to Mineralogy and Petrology, v. 107, p. 472–483.
Lasaga, A. C., 1979. Multicomponent Exchange and Diffusion in Silicates: Geochimica et Cosmochimica Acta, v. 43, p. 455–469.
——— 1983, Geospeedometry: an extension of geothermometry, *in* Saxena, S. K., editor, Kinetics and Equilibrium in Mineral Reactions: Advances in Physical Geochemistry, v. 3, p. 81–114.
Lasaga, A. C., Richardson, S. M., and Holland, H. D., 1977, The mathematics of cation diffusion and exchange between silicate minerals during retrograde metamorphism. *in* Saxena, S. K. and Bhattacharji, S., editors, Energetics of Geologic Processes: New York, Springer-Verlag, p. 353–388.
Lindstrom, R., Viitanen, M., Juhanoja, J., and Holtta, P., 1991, Geospeedometry of metamorphic rocks: examples in the Rantasalmi-Sulkava and Kiuruvesi areas, eastern Finland. Biotite-garnet diffusion couples: Journal of Metamorphic Geology, v. 9, p. 181–190.
Loomis, T. P., 1983, Compositional zoning of crystals: A record of growth and reaction history. *in* Saxena, S. K., editor, Kinetics and Equilibrium in Mineral Reactions: Advances in Physical Geochemistry, v. 3, p. 1–60.
Lovera, O. M., Richter, F. M., and Harrison, T. M., 1989, The $^{40}Ar/^{39}Ar$ thermochemistry for slowly cooled samples having a distribution of diffusion domain sizes: Journal of Geophysical Research, v. 94, p. 17917–17935.
——— 1991, Diffusion domains determined by argon-39 released during step heating: Journal of Geophysical Research, v. 96, p. 2057–2069.
Molnar, P., Chen, W., and Padovani, E., 1983, Calculated temperatures in overthrust terrains and possible combinations of heat sources responsible for the tertiary granites in the greater Himalaya: Journal of Geophysical Research, v. 88, p. 6415–6429.

Motoyoshi, Y., Thost, D. E., and Hensen, B. J., 1991, Reaction textures in calcsilicate granulites from the Bolingen islands, Prydz Bay, East Antarctica: Implications for the retrograde P-T path: Journal of Metamorphic Geology, v. 9, p. 293–300.
Nichols, G. T. and Berry, R. F., 1991, A decompression P-T path, Reinbolt Hills, East Antarctica: Journal of Metamorphic Geology, v. 9, p. 257–266.
Richter, F. M., Lovera, O. M., Harrison, T., and Copeland, P., 1991, Tibetan tectonics from argon-40/argon-39 analysis of a single potassium-feldspar sample: Earth and Planetary Science Letters, v. 105, p. 266–278.
Rubenach, M. J., 1992, Proterozoic low-pressure/high-temperature metamorphism and an anticlockwise P-T-t path for the Hazeldene area, Mount Isa Inlier, Queensland, Australia: Journal of Metamorphic Geology, v. 10, p. 333–346.
Sautter, V. and Harte, B., 1990. Diffusion gradients in an eclogite xenolith from the Roberts Victor kimberlite pipe: (2) kinetics and implications for petrogenesis: Contributions to Mineralogy and Petrology, v. 105, p. 637–649.
Selverstone, J., and Spear, F. S., 1985, Metamorphic P-T paths from pelitic schists and greenstones from the south-west Tauern Window, Eastern Alps: Journal of Metamorphic Geology, v. 3, p. 439–465.
Selverstone, J., Spear, F. S., Franz, G., and Morteani, G., 1984, High-pressure metamorphism in the SW Tauern Window, Austria: P-T paths from hornblende-kyanite-staurolite schists: Journal of Petrology, v. 25, p. 501–531.
Smith, D. and Barron, B. R., 1991, Pyroxene-garnet equilibration during cooling in the mantle: American Mineralogist, v. 76, p. 1950–1963.
Smith, D., and Wilson, C. R., 1985, Garnet-olivine equilibration during cooling in the mantile: American Mineralogist, v. 70, p. 30–39.
Spear, F. S., 1988, Metamorphic fractional crystallization and internal metasomatism by diffusional homogenization of zoned garnets: Contributions to Mineralogy and Petrology, v. 99, p. 507–517.
——— 1991, On the interpretation of peak metamorphic temperatures in light of garnet diffusion during cooling: Journal of Metamorphic Geology, v. 9, p. 379–388.
Spear, F. S., Kohn, M. J., Florence, F. P., and Menard, T., A model for garnet and plagioclase growth in pelitic schists: Implications for thermobarometry and P-T path determinations: Journal of Metamorphic Geology, v. 8, p. 683–696.
Spear, F. S., Peacock, S. M., Kohn, M. J., Florence, F. P., and Menard, T., 1991, Computer programs for petrologic P-T-t path calculations: American Mineralogist, v. 76, p. 2009–2012.
Spear, F. S. and Rumble, D. III, 1986, Pressure, temperature, and structural evolution of the Orfordville Belt, West-Central New Hampshire: Journal of Petrology, v. 27, p. 1071–1093.
Spear, F. S., Selverstone, J., Hickmott, D., Crowley, P., and Hodges, K., 1984, P-T paths from garnet zoning: a new technique for deciphering tectonic processes in crystalline terranes: Geology, v. 12, p. 87–90.
Tracy, R. J., 1987, Metamorphic Geology: Reviews of Geophysics, v. 25, p. 1115–1122.
Tracy, R. J., and Dietsch, C. W., 1982, High-temperature retrograde reactions in pelitic gneiss, central Massachusetts: Canadian Mineralogist, v. 20, p. 425–437.
Waldron, Kim Ann, ms, 1987, High Pressure contact metamorphism in the aureole of the Cortlandt Complex, southeastern New York, Ph.D. Thesis, Yale University.